CONTEXT-DEPENDENT VARIABILITY OF HIF HETERODIMERS INFLUENCES INTERACTIONS WITH MACROMOLECULAR AND SMALL MOLECULE PARTNERS

Joseph D. Closson[1,2], Xingjian Xu[1,2], Meiling Zhang[1], Tarsisius T. Tiyani[1,2], Leandro Pimentel Marcelino[1,3], Eta A. Isiorho[1], Jason S. Nagati[4,5], Joseph A. Garcia[4,5], Kevin H. Gardner[1,3,6,*]

*: direct correspondence to kgardner@gc.cuny.edu

[1]: Structural Biology Initiative, CUNY Advanced Science Research Center, New York, NY 10031
[2]: Ph.D. Program in Biochemistry, The Graduate Center – City University of New York, New York, NY 10016
[3]: Department of Chemistry and Biochemistry, City College of New York, New York, NY 10031
[4]: Department of Medicine, Columbia University Irving Medical Center, New York, NY 10032
[5]: Departments of Medicine and Research & Development, James J. Peters Veterans Affairs Medical Center, Bronx, NY 10468
[6]: Ph.D. Programs in Biochemistry, Biology, and Chemistry, The Graduate Center – City University of New York, New York, NY 10016

ORCIDs:
Joseph D. Closson: 0000-0002-4618-3119 / Xingjian Xu: 0000-0002-9609-4755 / Meiling Zhang: 0000-0002-0670-6018 / Tarsisius T. Tiyani: 0000-0002-2806-4079 / Leandro Pimentel Marcelino: 0000-0001-6067-0725 / Eta A. Isiorho: 0000-0002-6242-9297 / Jason S. Nagati: 0000-0002-4507-6581 / Joseph A. Garcia: 0000-0002-5621-7538 / Kevin H. Gardner: 0000-0002-8671-2556

Keywords: Hypoxia inducible factors (HIFs), aryl hydrocarbon receptor nuclear translocator (ARNT), clear cell renal cell carcinoma (ccRCC), hypoxia, transcription factors, small molecule binding, higher order complex formation

Running title: Variability of HIF complexes influences intermolecular interactions

Abstract

Hypoxia inducible factors (HIFs) are transcription factors that coordinate cellular responses to low oxygen levels, functioning as an α/β heterodimer which binds a short hypoxia response element (HRE) DNA sequence. Prior studies suggest HIF/HRE complexes are augmented by the binding of additional factors nearby, but those interactions are not well understood. Here, we integrated structural and biochemical approaches to investigate several functionally relevant HIF assemblies with other protein, small molecule, and DNA partners. First, we used cryo-electron microscopy (cryo-EM) to establish HIF-1 and HIF-2 form novel "dimer-of-heterodimers" (DoHD) complexes on extended human EPO enhancer sequences, showing that one heterodimer bound at a canonical HRE site with the second binding in an inverted fashion to an HRE-adjacent sequence (HAS) 8 bp away. Consistent with ARNT PAS-B domains predominating interactions within a DoHD, we found HIF-1 and HIF-2 assemble mixed DoHD complexes on the same DNA. Second, we saw substantial variability among ligands for isolated ARNT or HIF-2α PAS-B domains to bind larger complexes: for example, the ARNT PAS-B binding KG-548 and KG-279 ligands both bound the simpler HIF-2 heterodimer but exhibited differential binding to a HIF-2 DoHD. Finally, we combined cryo-EM and hydrogen-deuterium exchange by mass spectrometry (HDX-MS) to show how HIF-1 and HIF-2 heterodimers engage the transforming acidic coiled-coil containing protein 3 (TACC3) coactivator via both ARNT and HIF-α subunits, though this was unseen in the larger DoHD. Our findings highlight the importance of both molecular context and dynamics in biomolecular complex formation, adding to the complexities of potential regulation.

58 **Significance Statement**

59 Hypoxia inducible factors (HIFs) are transcription factors that regulate oxygen-dependent
60 cellular processes with implications in certain types of cancers. Current molecular structures of
61 HIFs bound to short DNA fragments provide insights into their function, but leave open
62 questions about how they bind longer natural DNA fragments and interact with small molecules
63 and protein coactivators. Integrating structural and biochemical techniques, we discovered a
64 novel assembly in which two HIFs bind together on a single extended DNA fragment, forming a
65 "dimer-of-heterodimers", and ascertained how structural differences arising from higher-ordered
66 complex formation affect ligand and coactivator binding. Our studies highlight how functional
67 contexts can shift structural paradigms and provide greater insight into the mechanisms by which
68 HIFs and similar transcription factors operate.

69

70 **Background**

71 The hypoxia inducible factors (HIFs) are basic helix-loop-helix Per-ARNT-Sim (bHLH-
72 PAS) transcription factors that regulate oxygen dependent processes for higher eukaryotes under
73 hypoxic conditions, controlling the expression of hundreds of genes in erythropoiesis, cell
74 growth, metabolism, and other pathways involved in adaptation to low oxygen levels (3, 10).
75 HIFs are heterodimers comprised of one of three isoforms of an oxygen-sensitive α-subunit
76 (HIF-1, 2, 3α) and a constitutively expressed β-subunit, aryl hydrocarbon nuclear translocator
77 (ARNT, also known as HIF-1β) (3, 11). Under normoxia, HIF-α subunits are degraded and
78 inactivated through O_2-dependent enzymatic hydroxylations of specific proline and asparagine
79 residues in the HIF-α C-terminus (4-6). These hydroxylation marks recruit the Von Hippel-
80 Lindau (VHL) E3 ubiquitin ligase (Pro-OH) and block recruitment of p300/CBP transcriptional
81 coactivators (Asn-OH), coordinately repressing HIF activity via independent mechanisms (3).
82 These hydroxylation events cannot occur under hypoxia, allowing HIF-α to accumulate, enter the
83 nucleus, and heterodimerize with ARNT, resulting in a HIF-α/ARNT complex (HIF complex)
84 bound to a 5 bp hypoxia response element (HRE) box (5'-RCGTG) in the promoter or enhancer
85 regions of oxygen-regulated genes to regulate transcription (**Fig. 1A**) (3, 10, 12, 13). DNA-
86 bound HIF complexes recruit other regulatory components such as p300 or CREB-binding
87 protein (CBP) coactivators, as well as a class of coiled-coil coactivators (CCCs), as integral parts
88 of transcriptional regulation (**Fig. 1**) (10, 14, 15).

89 Functionally, HIF-1 and 2 play major roles in natural cellular hypoxic responses, with
90 their dysfunction implicated in a range of cancers and other diseases (3, 10, 16-18). Though their
91 expression profiles tend to overlap, HIF-1 is typically associated with expression of glycolytic
92 enzymes ubiquitously, whereas HIF-2 is associated with expression of erythropoietin and

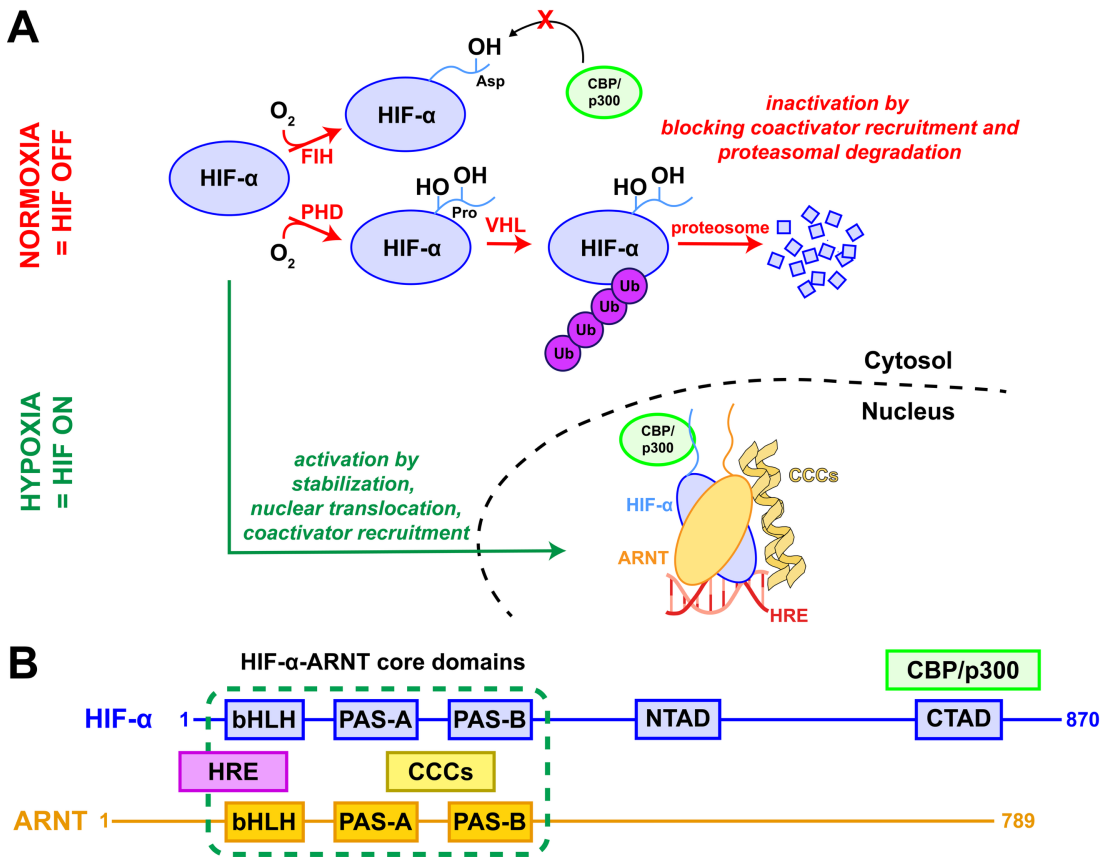

Figure 1. Schematic of HIF pathway regulation and components. (A) Under normoxic conditions, HIF-α is inactivated in the cytosol through parallel oxygen-dependent post-translational hydroxylations of residues in the protein C-terminus. These include a proline-directed mechanism (HIF-1α: Pro402 and 562, HIF-2α: Pro405 and 531) which leads to the recruitment of the von Hippel-Lindau E3 ubiquitin ligase, leading to poly-ubiquitination and proteosomal degradation (3, 4). A second route focuses on an asparagine residue (HIF-1α: Asn803, HIF-2α: Asn851) in the C-terminal transactivation domain (CTAD), preventing recruitment of CBP/p300 coactivators essential for HIF-driven transcriptional activation (5, 6). Under hypoxic conditions, neither of these HIF-α hydroxylations occur, allowing the fully functional protein to accumulate, translocate into to the nucleus, and heterodimerizes with ARNT. The HIF-α-ARNT complex then associates with specific HRE sequences in the promoter or enhancer regions of oxygen-dependent genes and recruits coactivators, leading to transcriptional activation. (B) Schematic depicting the domain arrangements of human HIF-2α and ARNT, as well as indicating which domains interact with HRE DNA as well as CCC- and CBP/p300-type transcriptional coactivators.

93 angiogenic genes localized to the kidney, lung, heart and small intestine (19, 20). Conversely,

94 HIF-3 has been implicated in fatty acid metabolism and potentially as a negative regulator of

95 hypoxic gene expression (21, 22). Constitutively high levels of HIFs can result in increased

96 levels of cellular growth, leading to tumorigenesis and specific types of cancers such as renal cell

97 carcinoma (HIF-2) and breast cancer (HIF-1), while the naturally hypoxic environment of tumors

98 can also upregulate HIF activity, exacerbating tumor progression through activation of hypoxic
99 pathways (10, 16-18, 23). Therefore, HIFs are an attractive target in the development of
100 anticancer agents with one such method of inhibition being the disruption of HIF-ARNT
101 complex formation, the proposed mechanism of action for the FDA approved HIF-2 inhibitor
102 and renal cell carcinoma/Von Hippel Lindau syndrome treatment, belzutifan (24-26).

103 Several protein/DNA crystal structures of bHLH-PAS transcription factors provide
104 structural insights into HIF/DNA binding interactions, most relevantly including several
105 structures of murine HIF-1 and HIF-2 bound to artificial 20 bp DNA fragments centered on
106 canonical 5 bp HRE boxes (5'-RCGTG) (9). Collectively, these structures show expected
107 bHLH/DNA interactions, as well as extensive association between the bHLH and PAS domains
108 on both protein subunits (**Fig. S1A,B**) (9). More broadly, this structural arrangement is highly
109 conserved among crystallographic and cryo-EM structures of various HIF complexes, as
110 swapping HIF-1/2/3α isoforms or ARNT homologs (to brain and muscle ARNT-like, BMAL1),
111 leads to only minor perturbations (**Fig. S1**) (9, 27, 28). Substantial changes in organization are
112 only seen with shifts of α subunits, as seen between HIF-2α/BMAL1 and CLOCK/BMAL1 (28,
113 29) complexes, which reorganize 4° arrangements of PAS domains within the heterodimer
114 assembly.

115 While these structural studies improved the understanding of protein/protein and
116 protein/DNA interactions in HIF complexes, several fundamental gaps in knowledge remain.
117 Foremost among these is the inability to explain long-standing data showing the importance of
118 DNA sequences adjacent to canonical HREs for HIF-driven transcriptional regulation. Initially
119 identified by deletion/mutation experiments of an enhancer region 3' to the human EPO gene,
120 full HIF-1 activity depends on the presence not only the HRE-box, but also an additional short

121 sequence (5'-CAC-3') 8 bp downstream, dubbed the HRE adjacent sequence (HAS) (13, 30).
122 Deletion or mutagenesis of the HAS markedly reduced HIF activity in cells (30); recent follow-
123 up studies showed that even minor changes to the length of the 8 bp HRE-HAS intervening
124 sequence similarly ablates HIF activity in cells, strongly implying cooperativity between these
125 regions (13, 30). While initially suggested that HAS sequences might function by recruiting a
126 separate transcription factor complex such as CREB-1/ATF-1, more recent studies suggest the
127 HAS might bind a second HIF heterodimer due to its similarity to the HRE (13, 31, 32). Such
128 higher order complexes have not been seen in existing structures of HIFs bound to short HRE-
129 only DNA fragments, leaving the arrangements of such higher-order HIF complexes an open
130 topic.

131 A second open area relates to the binding of small molecules within bHLH-PAS
132 complexes, which can naturally or artificially modulate their function. Most such compounds
133 bind within the PAS domains themselves, particularly into substantially-sized internal cavities
134 can exist (*e.g.* 100-500 $Å^3$ in HIF-α PAS-B domains (27, 33)), providing sites for specific
135 binding to disrupt protein/protein interactions. This strategy has been successfully used for the
136 HIF-2α specific inhibitor belzutifan, now clinically used to treat various forms of clear cell renal
137 cell carcinoma (19, 21, 24-26, 34). Additional binding sites are on PAS domain surfaces (1),
138 providing alternative routes to such regulation. However, almost all binding information on these
139 compounds have been determined on isolated PAS domains (1, 7, 35) or DNA-free bHLH-PAS
140 heterodimers (9, 24, 27). As such, substantive questions remain open about potential linkages
141 between small molecule binding into various HIF complexes.
142

143 Finally, questions remain open regarding interactions between the HIF-α/ARNT
144 heterodimer and other proteins involved in transcriptional regulation, such as transcriptional
145 coactivators. While some of these, such as p300/CBP, are well-known to interact with C-terminal
146 disordered regions in HIF-1α and HIF-2α (36), other coactivators are thought to directly interact
147 with the ordered bHLH/PAS core. These include the CCCs, three of which are known
148 components of ARNT-containing transcriptional complexes: transforming acidic coiled-coil
149 containing protein 3 (TACC3), thyroid hormone receptor/retinoblastoma interacting protein 230
150 (TRIP230) and coiled-coil coactivator (CoCoA) (2, 15, 37-39). Prior biochemical and structural
151 studies from our group suggested that ARNT/CCC interactions are driven by the ARNT PAS-B
152 domain binding to a C-terminal conserved "TACC box" in TACC3, CoCoA, and TRIP230 (14,
153 15, 37, 40). However, understanding how TACC boxes bind to bHLH/PAS heterodimers has
154 been complicated by the lack of characterization of CCC-bound bHLH/PAS complexes, as
155 studies on TACC/ARNT PAS-B complexes (including binding, NMR, and crystallographic
156 analyses (14, 15)) and crystal structures of CCC-free bHLH-PAS heterodimers (9) have
157 conflicting views of the accessibility of proposed binding sites.
158 Together, these results suggest that current structural models of HIF heterodimers may
159 not fully explain existing data about larger HIF complexes that form in different functional
160 contexts with additional DNA, proteins, or small molecules bound. To address this possibility,
161 we explored different HIF complexes using cryo-electron microscopy (cryo-EM) together with a
162 variety of biochemical and biophysical approaches. Specifically, we compared cryo-EM models
163 of human HIF-2 bound to either a synthetic 20 bp HRE fragment or extended DNAs from the
164 human EPO enhancer region which naturally contain both the HRE and HAS boxes. While we
165 observed a very similar HIF-2/HRE cryo-EM structure (3.61 Å) as previously seen by X-ray

166 crystallography, the longer HIF-2/HRE+HAS cryo-EM structure (3.74 Å) adopted a novel larger
167 configuration, with two individually assembled HIF-2 heterodimers binding each other
168 symmetrically while engaging the HRE and HAS boxes of a single DNA fragment. These larger
169 "dimer of heterodimer" (DoHD) complexes are chiefly mediated by ARNT-ARNT interactions
170 between the adjacent HIF-2 heterodimers, implying that they could form in other HIF complexes
171 as well. Consistent with this, we observed longer HRE+HAS DNAs efficiently forming similar
172 large complexes for HIF-1 and even mixed HIF-1/HIF-2 complexes. Additionally, we
173 investigated the ability of both HIF-2 complexes to bind small molecules known to bind isolated
174 HIF-2α and ARNT PAS-B domains, finding variability in binding which we attribute to more
175 dynamics within HIF complexes than appreciated to date. Finally, we propose a binding interface
176 for CCCs on HIF-1 and HIF-2 bound to 20 bp DNA fragments through cryo-EM modeling and
177 hydrogen-deuterium exchange mass spectrometry (HDX-MS). This binding, while observed in
178 heterodimers, is seemingly impaired in the larger DoHD complex, again suggesting differences
179 in dynamics among various complexes. Taken together, our findings suggest that the molecular
180 context of the bHLH-PAS HIF complexes can substantially modulate their abilities to bind other
181 functionally-important molecules which regulate their function.
182

183 **Results**

184 **Cryo-EM of HIF-2/HRE complexes show similar structures, but more dynamics, than**
185 **crystallographically**

186 Initially, we set out to determine a cryo-EM structure of human HIF-2 bHLH/PAS
187 heterodimers bound to a synthetic 20 bp HRE DNA fragment previously used for
188 crystallographic studies (9), mixed with C-terminal fragments of human TACC3 or CoCoA.

189 Such a structure would allow direct comparisons between these human complexes and prior
190 structures of murine proteins (**Fig. S1**) (9), while also giving insights into CCC binding modes.
191 The resulting datasets showed a high degree of heterogeneity, including a substantial number of
192 particles that appeared to be HIF-2 complexes without bound CCCs. Focusing first on these HIF-
193 2/HRE complexes, we used cryoSPARC (41, 42) to pick ~1,980,000 particles and progressively
194 filtered out undesired ones through iterative processes of 2D classification, *ab initio*
195 reconstruction, and 3D refinement (**Fig. S3**). We observed a mix of 2D class averages from this
196 analysis, including those clearly corresponding to HIF-2/HRE complexes like the prior crystal
197 structures (**Fig. 2A**). Intriguingly, we also saw classes that exhibited greater conformational
198 dynamics than previously reported, including those that appeared to be DNA-free (with
199 correspondingly disordered bHLH domains) and DNA-bound complexes with a detached or
200 blurred portion similar in size to a PAS domain (**Fig. 2B**). Given the organization of HIF
201 bHLH/PAS heterodimers, we interpret this as a ARNT PAS-B domain which has separated from
202 the rest of the HIF-2α/ARNT heterodimer.
203

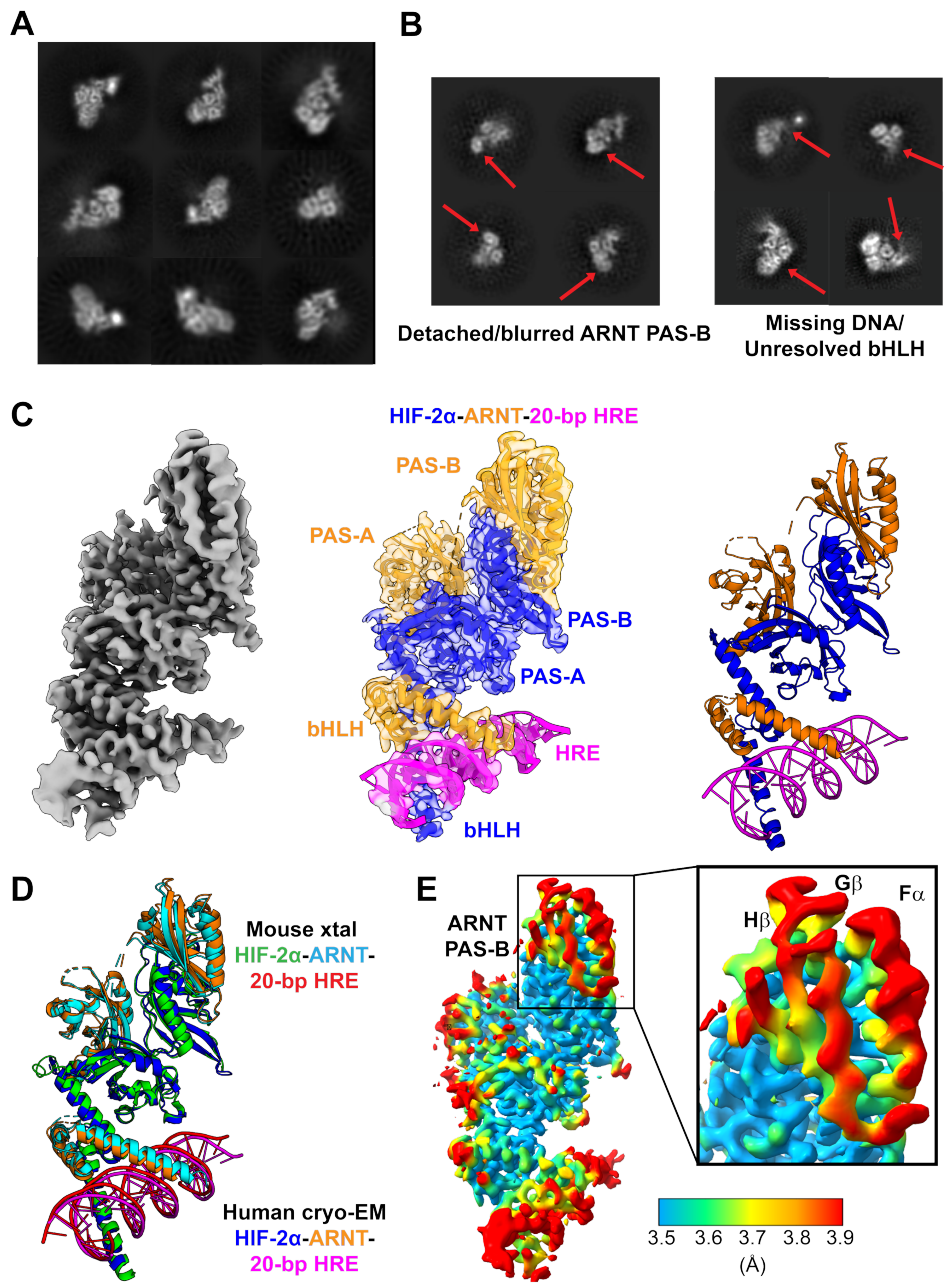

Figure 2. Cryo-EM structural analysis of human HIF-2 bound to 20 bp HRE fragments. (A) Cryo-EM 2D classes of HIF-2 complexes, with individual PAS and bHLH domains and DNA visible. (B) Some 2D classes of HIF-2 complexes showed either an apparent ARNT PAS-B detached from the rest of the HIF-2α-ARNT core (left) or destabilized bHLH domains lacking bound DNA (right). (C) 3.61 Å EM map (262,466 particles, 13.3% of all collected particles) was generated from refinement of the most populated *ab initio* volume into which an AlphaFold 2 model of human HIF-2 was fit. (D) Overlay of the mouse HIF-2 crystal structure (PDB code: 4ZPK, (9)) and human HIF-2 cryo-EM structure show highly similar domain architectures. (E) Local resolutions mapped onto the HIF-2 cryo-EM density map show a region of particularly low local resolution/high flexibility in the ARNT PAS-B (Fα-helix, Gβ-strand, Hβ strand) domain and bHLH domains.

205 Using ~262,000 particles (13.3% of the total particles picked) from the HIF-2/DNA class
206 noted above, we obtained a 3.61 Å EM map which we successfully fit with an AlphaFold-
207 generated model of human HIF-2α-ARNT-HRE DNA (**Fig. S4A**) without requiring any large-
208 scale rearrangements (**Fig. 2C**). Aside from the termini of the HRE fragment, which were not
209 well resolved in the cryo-EM map, fits between the model and experimental map were quite
210 good. Similar to HIF crystal structures (9, 27), several long protein loops were unresolved, with
211 the most notable being the ARNT PAS-A/PAS-B linker (ARNT residues 346-359), likely due to
212 high flexibility in these regions.

213 Notably, while our cryo-EM structure superimposed well with the murine crystal
214 structure, as expected from the > 95% sequence identities of the HIF-2α and ARNT bHLH/PAS
215 regions, we observed that the structures slightly differ in the location of the ARNT PAS-B
216 domains. This difference seems to be a domain-level shift of the cryo-EM ARNT PAS-B domain
217 away from the adjacent HIF-2α PAS-B domain and the rest of the heterodimer (**Fig. 2D**).
218 Supporting this, local resolution analysis of the cryo-EM map estimated most regions had
219 resolutions between 3.2-4.0 Å, with the lowest protein-associated resolutions corresponding to
220 the ARNT PAS-B domain and in some of the extended loops, again consistent with local
221 dynamics in these regions (**Fig. 2E**). Together with our observation of even larger movements of
222 ARNT PAS-B in the 2D class averages (**Fig. 2B**), we suggest that this domain has markedly
223 more dynamics than previously appreciated, with potential functional links we explore below.
224

225 **HIF2α-ARNT forms a heterotetrameric structure on EPO enhancer DNAs**

226 As noted above, previous studies indicated that additional DNA sequences adjacent to
227 HRE boxes are functionally important for full activation of certain oxygen-regulated gene

228 promoters (13, 30). To explore the structural basis of this observation, we used cryo-EM to
229 examine HIF-2 complexes bound to longer ~50 bp human EPO enhancer DNA sequences,
230 previously demonstrated to include both a HRE and HAS box used for full activation. Using
231 DNAs including both HRE and HAS boxes with additional flanking sequences on either the 5'
232 (dubbed BS1, 51 bp) or 3' (dubbed BS2, 52 bp) ends, we collected cryo-EM datasets of human
233 HIF-2 complexes bound to these longer DNAs, mixed with C-terminal TACC3 fragments. As
234 with our studies of the shorter 20 bp HRE complexes, most particles were TACC3-free, so we
235 focus here on complexes of HIF-2 bound to the 51 bp BS1 DNA fragments.

236 Early in our analysis, we observed 2D class averages that were markedly different than
237 seen for HIF-2α-ARNT bound to 20 bp HRE (**Fig. 3A**). Instead, we saw classes with much larger
238 protein density arranged more symmetrically about the DNA, prompting further structural
239 examination of these complexes. Final refinement of data from 164,000 particles (25.0% of all
240 particles picked) (**Fig. S5**), led to the determination of a 3.74 Å structure which neatly fit two
241 individually assembled HIF-2α-ARNT heterodimers as well as the 51 bp BS1 DNA fragment
242 into a "dimer-of-heterodimers" (DoHD) conformation within our density map without needing
243 any large scale domain rearrangement (**Fig. 3B**). We underscore DoHD complexes were
244 observed by size exclusion chromatography before freezing (**Fig. S6**) and we did not see any
245 comparable higher-order assemblies in our HIF-2/20 bp DNA cryo-EM results, supporting that
246 formation of this larger complex can occur *in vitro*, is dependent on the bound DNA component,
247 and is not an artifact of cryo-EM processing.

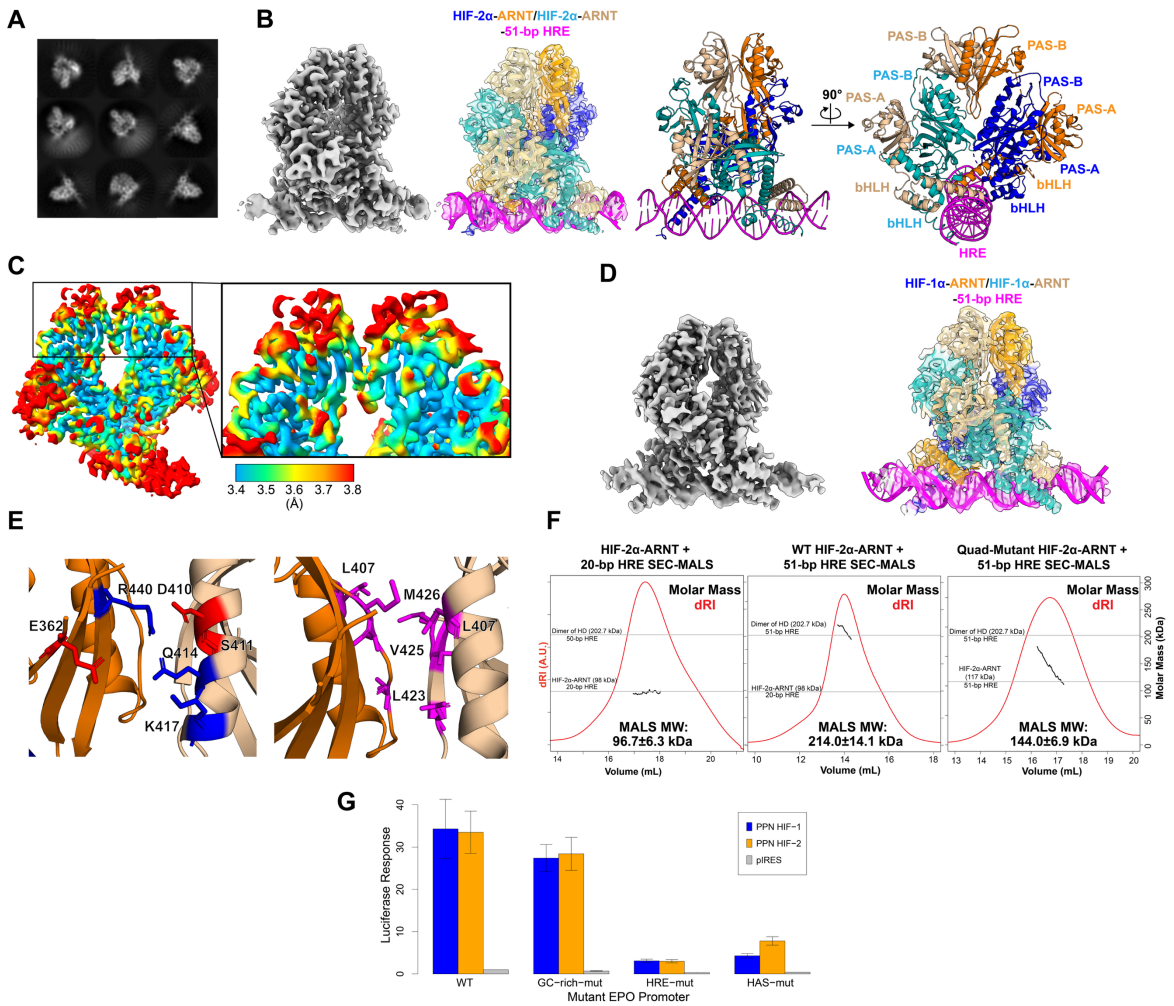

Figure 3. Structural and biochemical analyses of HIF dimer-of-heterodimer complexes. (A) 2D cryo-EM class averages from analyses of data collected on HIF-2α-ARNT heterodimers bound to 51 bp BS1 HRE/HAS DNA fragments, showing markedly different (and often, more symmetrical) arrangements than comparable 2D class averages of HIF-2 bound to 20 bp HRE DNAs. (B) A 3.74 Å EM map (164,352 particles, 25.0% of all collected particles) was generated from refinement of the most populated *ab initio* volume into which two individually assembled human HIF-2 heterodimers were fit, along with the corresponding 51 bp BS1 HRE/HAS DNA fragment. (C) Local resolution data mapped onto the HIF-2 dimer-of-heterodimers cryo-EM map showed that the ARNT PAS-B Fα-helix and Gβ-strand were higher relative resolution than in corresponding sections of the 20 bp HRE-bound HIF-2 EM map, suggestive of ordering between the heterodimer and dimer-of-heterodimer complexes. (D) The 3.90 Å cryo-EM map (71,802 particles, 27.3% of all collected particles) of HIF-1 bound to a 52 bp BS2 HRE/HAS DNA fragment showed a highly similar domain arrangement to HIF-2, though the ARNT PAS-A domains were less resolved. (E) Highlighted residues were suspected to form interactions between the opposing ARNT PAS-B domains in the HIF-2 supercomplex (basic residues in blue, acidic residues in red, uncharged residues in magenta) (F) SEC-MALS data showed expected differences in the molecular weights of HIF-2 on 20 bp HRE DNA fragments (96.7±6.3 kDa) and 51 bp BS1 HRE/HAS DNA fragments (214.0±14.1 kDa), but revealed an intermediate value (144.0±6.9 kDa) for a HIF-2 variant with mutations in four key ARNT PAS-B Fα-helix and Gβ-strand residues which are at the ARNT/ARNT interface essential to the dimer-of-heterodimers complex. (G) Luciferase reporter assays containing the wildtype (WT) or mutant versions of the human EPO enhancer with changes in the upstream GC-rich region (GC-rich-mut), HRE (HRE-mut), or HAS (HAS-mut) site were performed in HEK293T cells in conjunction with ectopic expression of oxygen-independent (PPN) HIF-1α or HIF-2α. Empty pIRES vector expression was measured to ensure empty vector would not contribute to reporter response. Mutations to either the HRE or HAS site substantially blunted reporter induction by either PPN HIF-1α and PPN HIF-2α.

248

249 This intriguing higher-order complex orients the two HIF-2 heterodimers around a
250 pseudo two-fold rotation axis, with one heterodimer ~180° rotated from the other. The first of
251 these heterodimers (1° heterodimer) bound to the HRE box through the HIF-2α and ARNT
252 bHLH domains as expected from the minimal complexes with 20 bp HRE-only DNAs. The 2°
253 heterodimer bound the HAS box through its respective bHLH domains (**Fig. 3B,S6**) from the
254 opposite side of the DNA as the 1° heterodimer, as expected from the spacing between the HRE
255 and HAS boxes. Protein/protein interactions between the two heterodimers were chiefly
256 mediated through the ARNT PAS-B domains, utilizing residues in the Fα-helix and Gβ-strand
257 with potential interactions between Leu407, Gln414, and Met426 of both ARNT PAS-B domains
258 that could be unambiguously placed at the protein/protein interface despite the limited resolution
259 of the cryo-EM map. Additional interactions may come from the HIF-2α PAS-A EF loops as
260 well (**Fig. S6**). Cryo-EM data for the central 27 basepairs of the 51 bp fragment were clearly
261 resolved to allow us to confidently place both the HRE and HAS boxes into the cryo-EM map,
262 with slight upward curvature in next to the HAS-box before losing resolution at the 3' terminus,
263 possibly supporting binding of the 2° heterodimer to the DNA.

264 We also performed local resolution analysis of this dimer-of-heterodimers cryo-EM map,
265 which spanned 3.2-4.2 Å resolution (**Fig. 3C**). While similar overall to our analysis from the 20
266 bp HRE-bound HIF-2, we observed two substantial changes. First, we saw higher resolution
267 density in the dimer-of-heterodimers map corresponding to the ARNT PAS-B domains
268 compared to the 20 bp HRE-bound HIF-2 map, specifically around the β-sheet surface and Fα-
269 helix located at the dimer/dimer interface. In contrast, the dimer-of-heterodimers map appears to
270 show relatively low resolution in the ARNT PAS-A domains of both heterodimers, likely due to
271 being distal to the protein/protein and protein/DNA interactions which stabilize the complex.

272

273 **Implications and validation of dimer-of-heterodimer assembly on other HIFs**

274 The central role of ARNT in mediating these dimer-of-heterodimer complexes has
275 several implications. First, analogous HIF-1 complexes should be able to form on longer DNAs,
276 given the shared role of ARNT in both HIF-1 and HIF-2. Second, point mutations at the ARNT
277 PAS-B domain, which provides the majority of protein/protein interface in the cryo-EM
278 structure, should destabilize dimer-of-heterodimer formation. Finally, "mixed" dimer-of-
279 heterodimers should be evident *in vitro*, combining HIF-1 and HIF-2 heterodimers bound to the
280 same DNA. We address each of these implications in turn below.

281 Starting with the ability of HIF-1 to form dimer-of-heterodimer structures, we collected a
282 cryo-EM dataset of human HIF-1 bHLH/PAS fragments bound to 52 bp BS2 HRE/HAS DNA
283 fragments, as initial characterization of HIF-1/DNA complexes appeared more homogenous with
284 BS2 (**Fig. S7**). 2D classes from this dataset were very similar to those from our prior HIF-2-BS1
285 studies above, suggesting similar structure formation (**Fig. S7B**). Further data refinement from
286 71,800 particles led to a 3.90 Å cryo-EM map, into which we could fit two individually
287 assembled HIF-1 AlphaFold-generated models using an inverted repeat-type arrangement as in
288 the HIF-2 dimer-of-heterodimers (**Fig. 3B,D; Fig. S6,S7**). As before, the ARNT PAS-B Fα-helix
289 and Gβ-strand elements appear to provide the bulk of protein/protein interaction surface within
290 the HIF-1 complex, consistent with the ARNT PAS-B domain playing a role in dimerizing HIF-1
291 as well as HIF-2. The HIF-1α PAS-A EF loops again appear to potentially play a further role in
292 stabilizing the DoHD complex, notably with apparent EM density between nearby cysteines
293 (Cys118) in these loops. While this implies the formation of a stabilizing disulfide bond in this
294 complex (**Fig. S7G**), its formation *in vivo* would likely require a change in the naturally reducing

295 cellular environment, such as could be achieved with increased reactive oxygen species (as
296 commonly seen in cancer cells where HIF-1 activity would be elevated (43)). Interestingly, the
297 ARNT PAS-A domains of this complex appeared to be of a much worse resolution than in the
298 HIF-2 DoHD complex, leading to fewer residues of this domain being confidently fit into the
299 EM map (**Fig. S7E**).
300

301 **The ARNT PAS-B domain serves as a major interface for HIF-2α-ARNT**
302 **homodimerization**

303 Our cryo-EM structures and local resolution analyses of the HIF dimer-of-heterodimers
304 support the ARNT PAS-B domain as a dimerization interface between the two HIF-α-ARNT
305 heterodimers (**Fig. 3B-D**). Independently, the ARNT PAS-B domain has been suggested to
306 participate in higher order HIF assemblies via analyses of intermolecular contacts in HIF crystal
307 structures (13), albeit in a different arrangement not supported by our cryo-EM structure. To test
308 the role of ARNT PAS-B a potential dimerization interface, we mutated specific residues at the
309 ARNT PAS-B/ARNT PAS-B interface of our dimer-of-heterodimer structure. These residues,
310 located in the ARNT PAS-B Fα-helix and neighboring β-strands, are both close to each other and
311 show improved local resolution in the dimer-of-heterodimers compared to the simpler
312 heterodimer structure, implying these regions are stabilized through direct interactions (**Fig. 3C**).
313 At this interface, we observed several sets of salt-bridges (Glu362 to Gln414/Lys417;
314 Asp410/Ser 411 to Arg440) and nonpolar clusters (Leu423 to Leu423; Met426 to
315 Leu407/Val425) (**Fig. 3E**) which are evolutionarily conserved among vertebrate ARNs (**Fig. S8**).
316 To disrupt these interactions, we mutated Glu362 and Arg440 to alanine and Leu423 and Met426
317 to lysine, developing a quad mutant ARNT (ARNT E362A/L423K/M426K/R440A) which we

318 predicted to have lower dimer-of-heterodimer stability than wildtype. Using size exclusion
319 chromatography coupled with multi-angle light scattering (SEC-MALS), we examined the
320 average molecular weights of the wildtype and mutant complexes with the 51 bp BS1 HRE/HAS
321 DNA fragment. For wildtype HIF-2, this complex had an average molecular weight of
322 214.0±14.1 kDa, similar to the expected 202.7 kDa for two HIF-2 heterodimers bound to a 51 bp
323 DNA duplex and effectively double the 96.7±6.3 kDa observed for a HIF-2 heterodimer bound
324 to a 20 bp HRE fragment (**Fig. 3F**). In contrast, HIF-2 containing the quad
325 E362A/L423K/M426K/R440A mutant ARNT bound to 51 bp BS1 DNA showed a later-eluting
326 SEC peak with an average 144.0±6.9 kDa molecular weight (**Fig. 3F**). Though higher than the
327 expected 117.0 kDa for a single HIF-2 heterodimer stably bound to a 51 bp DNA duplex, our
328 SEC and MALS data strongly support an equilibrium shift towards a single heterodimer.
329 Combining these results to the cryo-EM structure and local resolution analysis suggest the
330 importance of the ARNT PAS-B Fα-helix and adjacent β-strands as an interface in the formation
331 of dimer-of-heterodimers.
332

333 **ARNT-mediated formation of mixed HIF-1/HIF-2 dimers-of-heterodimers**

334 As the last of the three implications of our dimer-of-heterodimer structures, we asked if
335 the commonality of ARNT in mediating comparable HIF-1 and HIF-2 dimers-of-heterodimers
336 could facilitate HIF-1 and HIF-2 complexing together to form a "heterodimer-of-heterodimers"
337 complex on extended DNAs. To test this, we created a fusion protein of HIF-1α tagged on the N-
338 terminus with *E. coli* maltose binding protein (MBP) to increase its molecular weight by about
339 45 kDa, allowing us to distinguish HIF-1 and HIF-2 complexes by SDS-PAGE and size
340 exclusion chromatography.

341 After copurifying this MBP-tagged HIF-1 with untagged HIF-2, we bound them to 51 bp
342 BS1 HRE/HAS DNA fragments, and ran this mixed sample over SEC. We observed two peaks
343 in the resulting chromatogram (**Fig. S9A**), with SDS-PAGE analysis showing all three subunits
344 (MBP-HIF-1α, HIF-2α, ARNT) in the first, earlier-eluting peak and only HIF-2α and ARNT in
345 the later peak (**Fig. S9D**). This supports the formation of a tandem HIF-1/HIF-2 heterodimer-of-
346 heterodimers on an extended DNA fragment. Intriguingly, we did not see a peak corresponding
347 to MBP-HIF-1/MBP-HIF-1 heterodimers, which we would expect to form based on our cryo-EM
348 data and have confirmed through SEC of MBP-HIF-1 heterodimers bound to 51 bp HRE/HAS
349 DNA fragments (**Fig. S9A**).

350 To explore the DNA sequence requirements for forming these higher order structures, we
351 repeated these experiments using 51 bp BS1 DNA fragments with mutations into either the HRE
352 or HAS-box to reduce protein binding to those sites (**Fig. S9B**). As expected, mutation of the
353 HRE-box prevented almost any heterodimer formation, suggesting the HAS box alone is
354 insufficient to stably recruit either single heterodimers or dimer-of-heterodimers; protein that is
355 not bound to DNA cannot stably form heterodimers, and therefore elutes in the void (**Fig.**
356 **S9C,S9E**). In contrast, mutation of the HAS-box increased the presence of a later elution peak
357 we attribute to a single heterodimer on DNA, though dimer of heterodimer formation was
358 reduced but still evident (**Fig. S9C,S9E**).

359 Coupled with the inability to observe stable dimers-of-heterodimers on 20 bp HRE-only
360 DNAs (by either cryo-EM or X-ray crystallography), we interpret these data as giving us insights
361 into the coupled protein/protein and protein/DNA interactions needed to assemble higher-order
362 HIF complexes: HIF/HRE interactions are key for 1° heterodimer recruitment, with additional

363 DNA interactions – ideally from an appropriately-spaced HAS box – needed to stabilize the
364 presence of a 2° heterodimer (13).
365
366 **Formation of HIF dimer-of-heterodimers is important to cellular function**
367 Building on our observation of HIF dimers-of-heterodimers *in vitro*, we conducted
368 further studies to determine if these complexes would assemble in cells, and if they are
369 functionally relevant. We generated luciferase reporter plasmids driven by EPO enhancer region
370 sequences or variants containing mutations in the HRE, HAS or 5' GC-rich regions, and
371 cotransfected these into HEK293T cells together with expression plasmids for oxygen-invariant
372 "PPN" variants of human HIF-1α or HIF-2α. Examining luciferase expression from these cells,
373 we observed robust expression of the reporter genes driven by either the WT promoter or one
374 containing point mutations in the GC-rich region. In contrast, expression from plasmids with
375 HRE mutations was ablated by approximately 90%, as expected from the key role that HREs
376 play in recruiting HIFs. Notably, expression from HAS-mutated promoters was also substantially
377 decreased compared to WT controls, with approximately 70-80% decreased activity (**Fig. 3G**).
378 As neither mutation completely ablated HIF-dependent transcription of the reporter, we suggest
379 that either the HRE or HAS sequence on its own may still recruit a single heterodimeric
380 complex. Indeed, many HIF-regulated genes do not contain an HAS-box, and therefore function
381 by binding only the HRE-box (13, 44).
382
383 **Structural differences between HIF-2α-ARNT complexes leads to differential ligand**
384 **binding**

385 Our work demonstrates that differences in protein and DNA fragments of HIF complexes
386 can markedly impact the quarternary structures of these components. To explore the functional
387 impact of these changes on the binding of small molecules to various HIF complexes, we
388 measured the binding affinities of several previously identified compounds that bind within or
389 onto the surface of HIF-2α or ARNT PAS-B. Such compounds, which have been sought as leads
390 for disruptors of protein/protein interactions in HIFs, have typically been identified using
391 biophysical or biochemical approaches focused on ligand binding to isolated PAS-B domains (2,
392 7, 35). These compounds range in affinity from nanomolar (e.g. compound **2** binding to HIF-2α
393 PAS-B, K_d 81 nM (7)) to high micromolar (e.g. ARNT PAS-B binding KG-548 and KG-279 (1))
394 (**Fig. 4A**), but comparable measurements have typically not been available on larger complexes,
395 some of which occlude obvious access to binding sites on or inside of the PAS domain targets.
396 To address this shortcoming, we used microscale thermophoresis (MST) assays on several HIF-
397 2α or ARNT targeting ligands with the HIF-2 heterodimer and the dimer-of-heterodimers bound
398 to fluorescein (FAM)-labeled 20 bp HRE or 51 bp BS1 HRE/HAS DNA fragments.
399 The first of these compounds, KG-548, still bound the single HIF-2 heterodimer with
400 only a slight drop in affinity from the isolated ARNT PAS-B (K_d 348 μM ARNT PAS-B; ~ 800
401 μM HIF-2 heterodimer) despite its binding interface on the ARNT PAS-B surface being blocked
402 by the HIF-2α PAS-B domain in the heterodimeric complex (**Fig. 4B**). This observation suggests
403 some flexibility in the ARNT PAS-B conformation with respect to the rest of the heterodimer, as
404 supported by some cryo-EM 2D classes of the HIF-2 complex with the ARNT PAS-B domain
405 apparently detached from the other core domains (**Fig. 2B**), as well as the lower local resolution
406 of the ARNT PAS-B domain within the 3D heterodimeric complex. Consistent with this, we

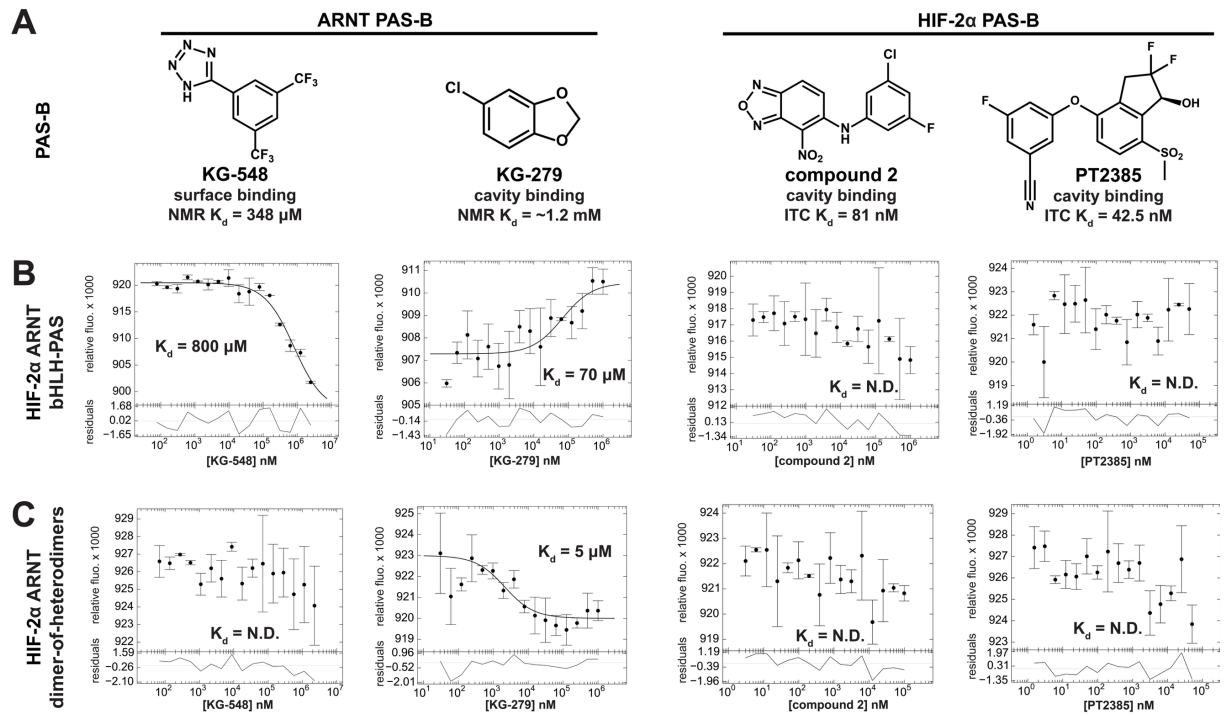

Figure 4. Contextual differences impact small molecule binding to ARNT and HIF-α PAS-B domains. (A) Known small molecule binders of isolated ARNT (KG-548 (1, 2), KG-279 (1, 2)) and HIF-2α PAS-B (compound 2 (7), PT2385 (8)) domains are shown along with their literature affinities for the specific PAS-B targets, obtained by microscale thermophoresis, ITC, and NMR. (B) Inclusion of the ARNT and HIF-2α PAS-B domains within a DNA-bound HIF-2 heterodimer substantially modulates binding affinities of PAS-B binding compounds compared to the free PAS-B domains, as assayed by MST with a fluorescein label attached to the 5' end of one strand of a 20 bp HRE duplex. (C) Incorporation of the PAS-B domains within a DNA-bound HIF-2 dimer of heterodimers further changes PAS-B ligand binding affinities, as detected with fluorescein label attached to the 5' end of one strand of a 51 bp BS1 HRE/HAS duplex.

found that KG-548 cannot bind the HIF-2 dimer-of-heterodimers complex (**Fig. 4C**), which has the ARNT PAS-B domains seemingly locked into place as they form key protein/protein interactions between heterodimers. We observed KG-279 binding to both HIF-2 bound to 20 bp HRE DNA fragments (**Fig. 4B**) and HIF-2 dimer-of-heterodimers on 51 bp BS1 HRE/HAS DNA fragments (**Fig. 4C**). Though binding to a single heterodimer would be expected due to observed flexibility of the ARNT PAS-B domain, binding to the larger dimer-of-heterodimers suggests the ARNT PAS-B internal cavity is accessible regardless of quaternary structure.

414 In contrast, we were unable to robustly observe binding in MST for compound 2 or
415 PT2385 to the HIF-2 heterodimer on 20 bp HRE or 51 bp HRE/HAS DNAs (**Fig. 4B,4C**). These
416 compounds bind to the internal cavities of the HIF-2α PAS-B domain, suggesting that the
417 pathways needed to access these cavities from solvent are blocked by heterodimerizing HIF-2α
418 and ARNT on a DNA template (45). This is especially intriguing since both compound 2 and
419 PT2385 disrupt HIF-2α and ARNT heterodimerization in cells (7), suggesting that this binds
420 HIF-2α prior to forming stable complexes on DNA.
421
422 **TACC3 interacts with loops of both HIF-α and ARNT subunits**
423 Though we can assemble dimer-of-heterodimers complexes on HRE/HAS DNA
424 fragments, we understand not all HIF-driven promoters contain both binding motifs. Therefore,
425 on alternative gene promoters, we suspect that HIFs may form varying higher-order complexes
426 with other parts of the transcriptional regulatory machinery. One well studied candidate for HIF
427 binding partners are the CCCs. While CCCs are clearly involved in transcriptional initiation from
428 HIF-driven promoters, and that this is mediated by direct interaction between HIF and CCC
429 proteins, the location of such interaction remains unclear. NMR and other biophysical data from
430 our lab suggested that CCCs bind to isolated ARNT PAS-B domains at a site (2, 15, 39)
431 inconsistent with subsequently-determined crystal (9) and cryo-EM (*vide infra*) structures of
432 larger HIF-2/HRE complexes.
433 To begin addressing this incompatibility, we sought to characterize larger HIF-2
434 complexes bound to CCCs. We purified C-terminal fragments of two CCCs, CoCoA and TACC3
435 (14, 15), confirmed that these were dimeric and coiled coil (**Fig. S10A,B**), and used MST to
436 measure the binding of these fragments to isolated ARNT PAS-B domains. We observed

437 micromolar affinities for these interaction, K_d 80 μM for CoCoA and 3 μM for TACC3 (**Fig.**
438 **5A**), consistent with prior results (14, 15). Repeating these measurements with the same CCC
439 fragments binding to HRE-bound HIF-2 complexes, however, showed K_d ~10 μM interactions of
440 both coactivators with HIF-2 (**Fig. 5B**), showing the involvement of additional regions outside of
441 ARNT PAS-B in the HIF-2α/ARNT heterodimer.

442 To obtain more structural insight into CCC/HIF-2 interactions, we added a TACC3
443 fragment (residues 758-838) to cryo-EM samples of HIF-2 bound to 20 bp HRE fragments. 2D
444 classes of this complex failed to resolve the HIF-2 protein domains, instead showing blurred
445 circular densities with "stick-like" objects protruding from them, which are of the right
446 dimensions to be TACC3 (**Fig. S10C**). Notably, of these classes showed a bend or break in the
447 stick-like density we attribute to TACC3, suggesting flexibility or dynamics within the
448 coactivator. This hypothesis was supported by a crystal structure of TACC3(758-838) (**Fig. 5C,**
449 **S10D**), which had low quality electron density and high B-factors for most residues N-terminal
450 of Lys788 (**Fig. 5C, Fig. S10D**), consistent with the break point seen in the cryo-EM classes.
451 Given this, we made a shorter TACC3(788-838) fragment ("shTACC3") which we utilized for
452 our subsequent biochemical and structural analyses. MST binding analysis of shTACC3
453 fragment titrated into HIF-2/HRE complex showed a 26 μM affinity (**Fig. 5C**), slightly
454 weakened from the longer 758-838 construct.
455

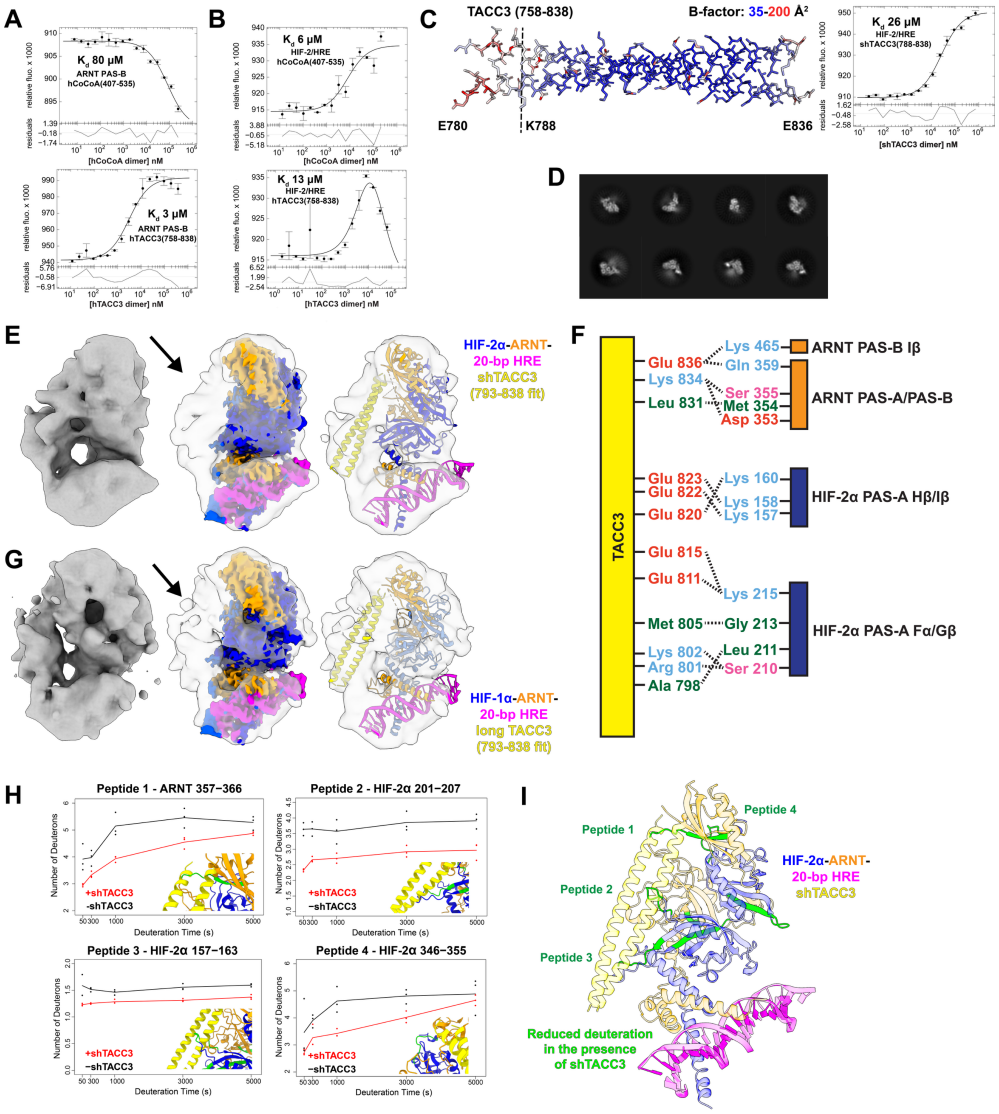

Figure 5. Coiled-coil coactivator binding to HIF heterodimers. (A, B) MST measurements of C-terminal fragments of CoCoA(407-535) and TACC3(758-838) binding to the (A) isolated ARNT PAS-B domains and (B) HIF-2α-ARNT heterodimers (HIF-2) bound to 20 bp HRE fragments. The two highest points of the hCoCoA to HIF-2 binding curve showed evidence of aggregation and were removed. TACC3 binding to HIF-2 showed a decrease at high concentration, suggesting a second binding mode or aggregation. (C) A truncated TACC3(788-838, "shTACC3") was designed based on our TACC3(758-838) crystal structure showing highly elevated B-factors and poor electron density in residues 758-788. This CCC fragment bound a 20 bp HRE-bound HIF-2 with a minimal affinity drop from the longer TACC3 (K_d 26 μM by MST), and without the secondary binding mode seen for longer fragments to HIF-2. (D) 2D classes of shTACC3 bound to 20 bp HRE-bound HIF-2 showed visible core domains with excess blurred density extending out of the central region. (E) *Ab initio* reconstruction of 20 bp HRE-bound HIF-2 bound to shTACC3. HIF-2 fit into the volume without major rearrangement, leaving excess density along the ARNT PAS-B/HIF-2α PAS-A interface for most of shTACC3 to be fit. (F) Schematic of interactions between TACC3(788-838) and HIF-2 shows three PAS domains interacting with the TACC3 coiled coil. Residues indicated on TACC3 originate from either chain. (G) Cryo-EM of HIF-1 bound to the longer TACC3(758-858) fragment showed similar excess density as HIF-2/TACC3(788-838), consistent with TACC3 binding similarly to HIF-1 and HIF-2. TACC3 residues 793-838 were confidently fit into the excess density for both HIF-1 and HIF-2. (H) HDX-MS deuterium uptake plots showed several HIF-2α and ARNT loops with increased protection from solvent in the presence of TACC3. (I) Mapping peptides with TACC3-induced HDX changes onto shTACC3-bound HIF-2 model (increased protection in green) showed these protected loops along the proposed TACC3 binding interface from cryo-EM.

456

457

458 Having confirmed *in vitro* binding on shTACC3 to HIF-2/HRE complexes, we collected
459 a cryo-EM dataset to obtain structural information on this activator/coactivator complex. Using
460 3,320,000 particles from this dataset, we proceeded with 2D classification and observed classes
461 with visible core domains of HIF-2 as well as blurred excess density which we attributed to
462 shTACC3 (**Fig. 5D**). *Ab initio* reconstruction from 222,000 particles led to a low resolution cryo-
463 EM density map (**Fig. S11**) in which we were able to loosely fit our cryo-EM structure of HIF-2
464 bound to 20 bp HRE. This fitting left additional unoccupied density alongside the ARNT PAS-B
465 and HIF-2α PAS-A domains (**Fig. 5E**). Into this region, we fit an AlphaFold structure of the C-
466 terminal 46 residues of shTACC3 as a dimeric coiled coil (**Fig. S5C**) with the C-termini facing
467 the ARNT PAS-B domain, as suggested by our prior work (14, 15). This density became more
468 diffuse towards the shTACC3 N-termini, consistent with the 2D class averages of longer
469 TACC3/HIF-2 complexes and our crystal structure. This structural model places shTACC3
470 adjacent to the HIF-2 PAS domains, suggesting shTACC3 interacts via charge/charge and
471 hydrophobic interactions with HIF-2 through unresolved loops in the ARNT PAS-B and HIF-2α
472 PAS-A domains (**Fig. 5F**) and explaining the differences in affinity we observed for TACC3
473 binding to ARNT PAS-B and larger HIF-2 complexes. Parallel cryo-EM studies of complexes of
474 the longer TACC3(758-838) bound to HIF-1/HRE showed TACC3-associated density in a
475 comparable spot relative to the HIF heterodimer, suggesting comparable binding interfaces
476 between the two isoforms (**Fig. 5G**).

477 While these independent observations of a common TACC3 binding site despite
478 differences in HIF-α isoform and TACC3 construct bolstered our confidence in their validity, we
479 sought independent confirmation from HDX-MS on HIF-2/HRE complexes in the absence and

480 presence of shTACC3. Comparing these data, we identified several HIF-2α and ARNT peptides
481 with notably less deuteration in the presence of shTACC3, most of which were along the
482 TACC3-binding interfaces seen in cryo-EM. Integrating the cryo-EM and HDX-MS results, we
483 found four loops in the proposed CCC binding interface supported by both methods (**Fig. 5H,I**):
484 ARNT PAS-A/B linker (357-366), HIF-2α PAS-A Fα/Gβ loop (157-163), HIF-2α PAS-A Hβ/Iβ
485 loop (201-207) and HIF-2α PAS-B C-terminal loop (346-355). We also observed several HIF-2α
486 peptides with TACC3-induced protection from HDX exchange at sites remote from the proposed
487 binding site, suggesting long-range stabilization of the HIF-2α/ARNT heterodimer upon CCC
488 binding (**Fig. 5I**).

489 As previously mentioned, we were unable to see TACC3 binding to the HIF-2 dimer-of-
490 heterodimers via cryo-EM, despite the presence of the CCCs on the grids. We performed
491 microscale thermophoresis to further probe interactions between TACC3 and the HIF-2 dimer-
492 of-heterodimers complex, but were again unable to see binding, prompting us to believe TACC3
493 cannot bind the larger complexes. Notably, the HIF-2α and ARNT loops we saw as critical for
494 binding appear to be unobstructed in the HIF-2 dimer-of-heterodimers complex, leading us to
495 suspect that differences in the dynamics (such as those suggested by differences in cryo-EM
496 local resolution) may contribute to this finding.

497

498 **Discussion**

499 HIFs have been implicated in specific types of cancer and the progression of
500 tumorigenesis, making them a target for anticancer therapeutics (16, 17, 25, 26). Successfully
501 developing such drugs, including the HIF-2α inhibitor belzutifan, required a mix of approaches
502 applied to reductionist models of HIF-α and ARNT components ranging from isolated PAS

503 domains to DNA-bound single bHLH/PAS heterodimers. While these approaches were
504 obviously successful at informing both basic science and applications of HIF biology, they left
505 unexplained prior findings in three areas – larger DNAs, small molecule binding, and CCC
506 binding – which we advance here.

507 The formation of higher-ordered HIF complexes was first suggested by Semenza and
508 Wang alongside their discovery of HIF-driven gene expression, and has been recently bolstered
509 by cellular and biochemical work from Rosell-Garcia *et al.* demonstrating that HRE or HAS
510 mutations within HIF-driven promoters drastically reduce HIF activity in cells, similar to our
511 results in **Fig. 3G** (13, 30, 46). Using a split-enzyme reconstitution assay, these authors also
512 nicely demonstrate the likely formation of DoHD complexes in cells. Taken together, HIF-driven
513 transcription clearly occurs from HRE-only or HRE/HAS-containing promoter/enhancer
514 sequences, with likely different dependencies on concentrations of HIF-α and ARNT subunits.
515 Rosell-Garcia *et al.* proposed that larger HIF complexes would form through interactions
516 between ARNT PAS-B and bHLH domains of interacting heterodimers, as suggested through
517 HIF crystal contacts. Such an arrangement places the two sets of bHLH DNA binding domains
518 relatively far from each other, requiring substantial distortion to bind a single DNA containing
519 HRE and HAS boxes.

520 In contrast, our DoHD complex places two HIF heterodimers in a symmetric arrangement
521 via the ARNT PAS-B β-sheet surfaces, with two sets of DNA binding domains ideally placed to
522 contact HRE and HAS boxes with the optimal 8 bp spacer, and not ones with shorter or longer
523 separations (13). Notably, little rearrangement of the HIF heterodimer is required to assemble
524 these larger dimer-of-heterodimer assemblies, in stark contrast to CLOCK/BMAL1: Higher-
525 order assemblies of HIF do not substantially alter HIF heterodimer structure upon dimerization,

526 while CLOCK/BMAL1 heterodimers undergo a dramatic 90° intramolecular pivot as they go
527 from isolated heterodimers to a nucleosome-bound complex (**Fig. S12**). Our model also explains
528 mutation data from Rosell-Garcia showing that intact ARNT PAS-B domains are required for
529 higher-order HIF complexes to form *in vitro* or in cells. Further, the high conservation of the
530 ARNT PAS-B domain, including residues involved in DoHD interactions, through vertebrates
531 suggests that such complexes are likely to be found across a wide variety of vertebrates (**Fig.**
532 **8C**). As such, we suggest that our dimer-of-heterodimers model best explains a variety of
533 biochemical and molecular data on interactions and functional importance of these higher-order
534 HIF structures.

535 Categorization of different promoters with HRE-only or HRE/HAS combinations reveals
536 that the latter group are largely involved in cell proliferation, metabolism and angiogenesis,
537 while HRE-only containing genes share these functions along with others including transcription
538 regulation, pH regulation, signaling and drug resistance (3, 44). HIFs have about a 2-3-fold
539 higher affinity for the HRE-box alone in comparison to the HRE/HAS-boxes together (13),
540 suggesting a dose dependence in which the formation of higher-ordered complexes, and
541 therefore the expression of HRE-only or HRE/HAS-containing genes, depends upon HIF
542 concentration (**Fig. 6**). This is supported by data from transfection-based control of HIF levels
543 for cells grown in culture (13), but yet to be demonstrated *in vivo* or with natural or artificial
544 regulators of HIF complexes.

545 The dimer-of-heterodimers concept also strongly suggests the potential for mixed HIF-
546 1/HIF-2 complexes controlling transcription as well as more canonical HIF-1/HIF-1 or HIF-
547 2/HIF-2. Since we have determined both HIF-1 and HIF-2 can form mixed dimer-of-heterodimer
548 complexes together on the same DNA fragment, the two isoforms likely engage in crosstalk to

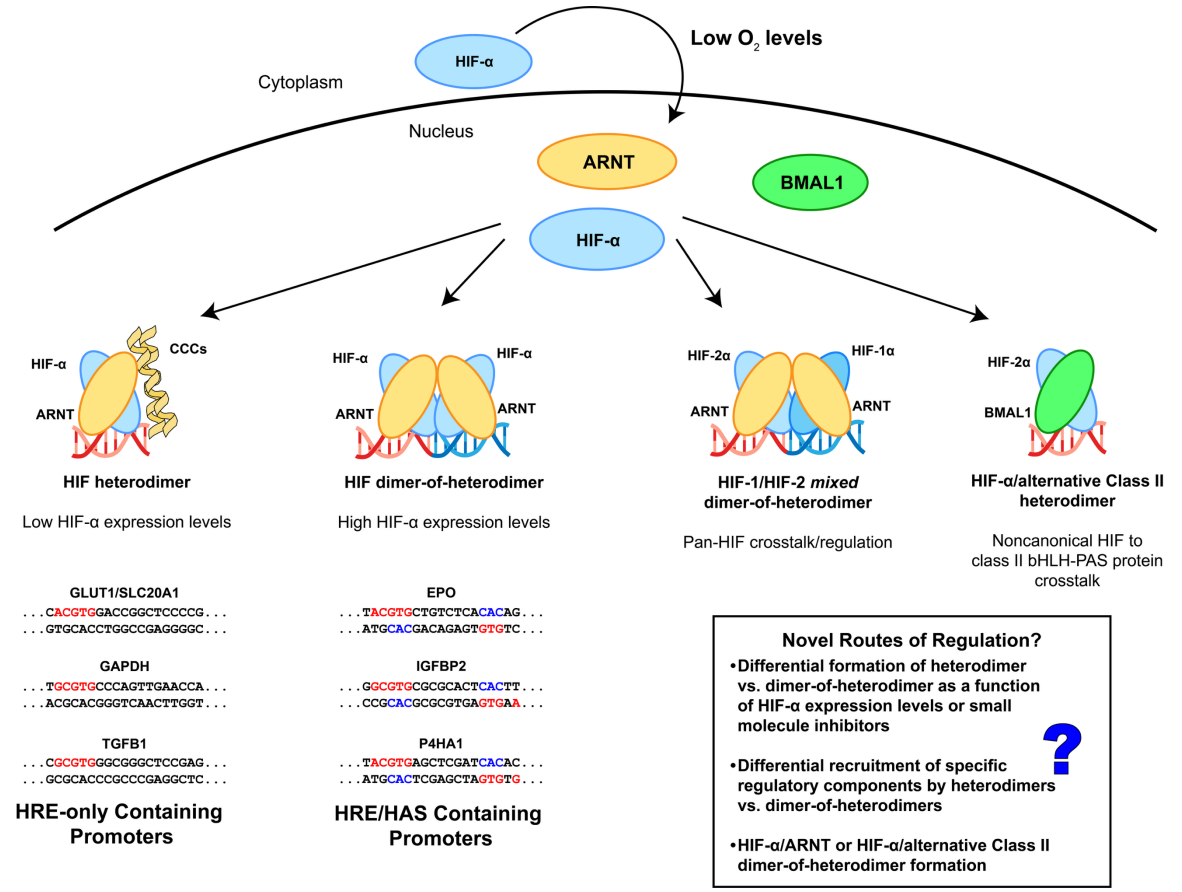

Figure 6. Proposed promoter-dependent formation of higher-order HIF and their downstream effects. (A) Under hypoxic conditions, we propose HIFs form different complexes based on the sequence of the promoter/enhancer region of the gene of interest. For HRE-only containing genes, we propose HIFs form a single heterodimer on the HRE-box, recruiting other components such as CCCs. For genes containing an HRE-box followed by an 8 bp spacer and an HAS-box, we propose that HIFs instead form a dimer-of-heterodimers. We suggest the specification of which genes are activated by HIF are dose dependent, in that lower cellular levels of HIF will activate HRE-only genes while higher cellular levels of HIF will activate HRE/HAS containing genes. Additionally, HIF-α can form noncanonical complexes with alternative class II bHLH-PAS proteins, including BMAL1, as well as mixed HIF-1/HIF-2 dimer-of-heterodimer complexes, each under varying conditions. We suggest that the similar quaternary structure of the HIF-2α-BMAL1 complex lends itself to the potential formation of dimer-of-heterodimers structures, though this remains to be experimentally validated.

549 regulate overlapping gene expression. Mixed dimer-of-heterodimer formation may also serve as
550 a mechanism of rescue in cases where either HIF isoform is depleted, either through natural or
551 artificial means (*e.g.* belzutifan inhibition of HIF-2). Rescue of either HIF isoform has been seen
552 in cases where HIF-1 is inactivated, HIF-2 activity will increase to compensate (47, 48); we
553 propose that part of this mechanism may be in the substitution of heterodimers in dimer-of-
554 heterodimer complexes. This raises the potential of other bHLH/PAS heterodimers to join in

555 higher order complexes. Recent cryo-EM of HIF-2/BMAL1 adopts a similar heterodimer dimer
556 structure as HIF-2/ARNT, and exposes a similar surface on the BMAL1 PAS-B as used in
557 ARNT PAS-B (49), raising the potential of other mixed higher-order complexes (**Fig. 6**).
558 Support for this concept is provided by a sequence alignment of the human ARNT,
559 BMAL1 and ARNT2 PAS-B domains, showing that while few residues along the DoHD
560 interface are conserved, though three such conserved sites, E362, Q414, and R440, are important
561 to DoHD formation (**Fig 3E,F;Fig. S8A,B**). With this, we suggest that dimer-of-heterodimer
562 formation may plausibly include other bHLH-PAS transcription factors provided that they adopt
563 a similar quaternary structure to HIF. For example, CLOCK-BMAL1 heterodimer structures do
564 not appear to be compatible with joining HIF/ARNT heterodimers based on existing structures,
565 although some evidence of CLOCK/BMAL1 higher order complexes have been seen in
566 structural studies of nucleosome-associated structures (28, 50).
567 Switching from the self-assembly of HIF-2α and ARNT to their ability to bind small
568 molecule ligands, our data clearly indicates that this binding interaction heavily depends on the
569 nature of the HIF-2α and ARNT assemblies. We have previously found a slate of small
570 molecules which can bind the isolated HIF-2α or ARNT PAS-B domains (e.g. compound 2 (7),
571 PT2385 (8), KG-548 (1, 2), KG-279 (1, 2)) as assessed by NMR, ITC, or MST. Some of these
572 compounds do not appear capable of binding DNA-bound HIF-2α-ARNT heterodimers on either
573 the short 20 bp HRE-only or longer 51 bp HRE-HAS constructs. This result suggests that the
574 internal PAS-B cavities are inaccessible to solvent in these higher-order assemblies, likely to due
575 to PAS/PAS interactions. Of note, the HIF-2α PAS-B binding compound 2 and PT2385 (7, 8)
576 inhibit HIF-2 driven transcription in cells, suggesting that the cavity is still accessible under
577 certain conditions. We suggest that this may happen in DNA-free HIF-2α/ARNT heterodimers,

578 as supported by the crystal structure of PT2385, a belzutifan precursor, bound to the HIF-2
579 heterodimer without any DNA present (24). This implies that belzutifan-type compounds may
580 need to inhibit HIF-2α-ARNT dimerization *before* DNA binding, which in turn stabilizes the
581 complex enough to prevent inhibitor binding or complex dissociation.

582 Notably, not all small molecule compounds we tested were incapable of interacting with
583 DNA-bound HIF-2α-ARNT heterodimers. Our examinations of KG-548, a small molecule that
584 binds the beta-sheet surface of ARNT PAS-B, shows that it clearly binds single HIF-2α-ARNT
585 heterodimers bound to a short HRE-only DNA, despite the fact that its binding surface on ARNT
586 PAS-B is occluded in both our cryo-EM and prior crystallographic structures of these complexes
587 (1, 9). We view this result as strongly suggesting the ARNT PAS-B domain having more
588 flexibility than evident in these static structures, as supported by the relatively low local
589 resolution of this domain in the single heterodimer/DNA complex and our observation of 2D
590 classes where the ARNT PAS-B seems to have detached from the result of the heterodimer.
591 More broadly, studies of other bHLH/PAS transcription factors show that the ARNT PAS-B
592 domain (or its analog in BMAL1) adopt a very diverse set of conformations with respect to
593 different Class I heterodimerization partners (HIF-α, AHR, NPAS, CLOCK), supporting this
594 hypothesis (9, 29, 51, 52). Notably, the dimer-of-heterodimers HIF-2α/ARNT structure, which
595 involves reciprocal interactions between ARNT PAS-B domains on adjacent heterodimers, is
596 incapable of binding as expected from squelching this inherent flexibility. Intriguingly, the fact
597 that KG-279, an ARNT PAS-B cavity binder, bound to both the HIF-2 heterodimer and dimer-
598 of-heterodimer complexes implies that rearrangement is not totally restricted as necessary
599 conformational changes needed to allow small molecules into the ARNT PAS-B cavity can still
600 occur, even in the larger dimer-of-heterodimers (1).

601 Finally, our work here sheds some much needed light on the nature of interactions
602 between CCCs and the HIF-α/ARNT heterodimers. While past work established the importance
603 of these interactions in HIF-driven transcriptional activation via ARNT (14, 40, 53-57), prior
604 work from our lab and others led to different, and conflicting, views as to the structural basis of
605 activator/coactivator recruitment (2, 9, 15, 39). Our complexes here of HIF-1 and HIF-2 bound to
606 different TACC3 fragments resolve this dilemma, showing a conserved interaction between the
607 C-terminus of TACC3 with ARNT PAS-B. Additional interactions are indicated by cryo-EM
608 (and HDX-MS for HIF-2), showing the involvement of loops on the HIF-α subunit. Notably, the
609 HDX-MS data shows a clear stabilization of the ARNT PAS-A/PAS-B linker upon TACC3
610 binding; a similar stabilization has been observed with a HIF-2 binding small molecule activator
611 (24), raising the question about similar activation modes despite the differences in activator
612 binding to the HIF heterodimer.

613 We close by underscoring that structural biology – like all experimental methods – has its
614 fundamental strengths and weaknesses. Within HIF biology, the strengths are clear as evidenced
615 by mechanistic understanding of how natural O_2 regulation is achieved, how disease-associated
616 disruptions have their effects, and how small molecules can be used therapeutically to target
617 those diseases. However, we equally see reminders that single structures of complexes, while
618 extremely useful on their own, may not entirely represent protein assemblies in their true
619 functional contexts, due either to experimental choice (e.g. selection of proteins, DNAs, small
620 molecules) or experimental liabilities (e.g. presence or absence of protein dynamics). With
621 additional HIF interacting partners to be discovered in genomic and broader contexts (28, 58),
622 there is more to discover.

623

624 **Materials and Methods**

625 **Cloning and Expression of HIF Complexes**

626 6xHis-tagged wildtype human HIF-2α (residues 5-361) or HIF-1α (residues 4-361) and untagged
627 human ARNT (residues 91-470) were cloned into a pETDuet-1 vector. HIF-α (6xHis-tagged)
628 and ARNT were coexpressed in BL21-CodonPlus (DE3) *E. coli* (Agilent) in Lysogeny Broth
629 with 0.1 mg/mL ampicillin and 0.034 mg/mL chloramphenicol. Cells were grown at 37°C and
630 induced with 0.5 M isopropyl-β-D-thiogalactopyranoside (IPTG) upon reaching an OD_{600} of 0.8-
631 1.0, then brought to 18°C to induce overnight (16-18 hr). Cells were harvested by spinning at
632 4°C and 4658xg for 30 min, resuspended in lysis buffer (50 mM HEPES (pH 7.4), 300 mM
633 NaCl, 3 mM β-mercaptoethanol (BME), 1 mM phenylmethylsulfonyl fluoride (PMSF), 0.1
634 mg/mL lysozyme and 0.01 U/mL benzonase nuclease), flash frozen and stored at -80°C.

635

636 **Cloning and Expression of Coiled-Coil Coactivators**

637 Wildtype human TACC3 (residues 758-838 or residues 788-838 [shTACC3]) or wildtype human
638 CoCoA (residues 407-535) were cloned into a pHis-GB1 vector. CCCs were then expressed in
639 BL21 (DE3) *E. coli* (Agilent) in Lysogeny Broth with 0.1 mg/mL ampicillin. Cells were grown
640 at 37°C and induced with 0.5 M isopropyl-β-D-thiogalactopyranoside (IPTG) upon reaching an
641 OD_{600} of 0.8-1.0, then brought to 18°C to induce overnight (16-18 hr). Cells were harvested by
642 spinning at 4°C and 4658xg for 30 min, resuspended in lysis buffer (50 mM Tris (pH 7.4), 150
643 mM NaCl, 1 mM PMSF 0.1 mg/mL lysozyme and 0.01 U/mL benzonase nuclease), flash frozen
644 and stored at -80°C.

645

646 **Purification of HIFα-ARNT Heterodimers**

647 Frozen HIF-1 or HIF-2 cell pellets were thawed, lysed by sonication and centrifuged at 47850xg
648 for 45 min. HIF-α-ARNT was purified using an AKTA Püre (Cytiva) by flowing lysate over a 5
649 mL HisTrap HP (Cytiva), followed by wash buffer (50 mM HEPES (pH 7.4), 300 mM NaCl, 20
650 mM imidazole, 2 mM BME) with stepwise increasing concentrations of imidazole (20-260 mM)
651 to remove nonspecifically bound protein. 6xHis-tagged HIF-α (bound to ARNT) was eluted with
652 elution buffer (50 mM HEPES (pH 7.4), 300 mM NaCl, 500 mM imidazole, 2 mM BME), mixed
653 with about a 20x molar excess of annealed DNA (20 bp, 51 bp BS1 or 52 bp BS2, IDT) and 5
654 mM $MgCl_2$ and allowed to bind for at least one hour at 4°C. Protein was then concentrated about
655 10x by dialyzing (3.5 kDa MWCO dialysis tubing, ThermoFisher) against dry polyethylene
656 glycol 35000. HRE-bound HIF-α-ARNT complexes were then further purified through a
657 Superdex 200 increase 10/300 analytical size exclusion column (Cytiva) with the final analytical
658 buffer (50 mM HEPES (pH 7.4), 250 mM NaCl, 5 mM $MgCl_2$). Protein samples were used
659 immediately or stored at 4°C for a maximum of 48 hr.
660 20 bp HRE: GGCTGCGTACGTGCGGGTCGT
661 51 bp BS1 HRE:
662 AGGGGTGGAGGGGGCTGGGCCCTACGTGCTGTCTCACACAGCCTGTCTGAC
663 52 bp BS2 HRE:
664 TGGGCCCTACGTGCTGTCTCACACAGCCTGTCTGACCTCTCGACCCTACCGG
665
666 **Purification of Coiled-Coil Coactivators**
667 Frozen cell pellets were thawed, lysed by sonication and centrifuged at 47850xg for 45 min.
668 TACC3 or CoCoA were purified using an AKTA Püre (Cytiva) by flowing lysate over a 5 mL
669 HisTrap HP (Cytiva), followed by wash buffer (50 mM Tris (pH 7.4), 150 mM NaCl, 20 mM

670 imidazole) with stepwise increasing concentrations of imidazole (39-106 mM) to remove
671 nonspecifically bound protein. 6xHis-tagged-GB1-CCC (TACC3 or CoCoA) was eluted with
672 elution buffer (50 mM Tris (pH 7.4), 150 mM NaCl, 500 mM imidazole) and diluted 1:10 in
673 TEV buffer (50 mM Tris (pH 7.4), 0.1 mM EDTA) with a 3:1000 addition of TEV protease to
674 cleave the His and GB1-tags from the protein. Cleaved tags were then removed by flowing the
675 protein over a 5 mL HisTrap HP to separate them from the protein of interest. CCC-containing
676 fractions were then concentrated about 15x using a 10 kDa MWCO Millipore centrifugal filter
677 unit (Sigma-Aldrich) at 1200xg and 4°C. Concentrated protein was further purified through a
678 Superdex 200 increase 16/40 HiScale size exclusion column (Cytiva) with the final analytical
679 buffer (50 mM HEPES (pH 7.4), 50 mM NaCl, 5 mM $MgCl_2$). Protein samples were used
680 immediately or stored at 4°C for a maximum of 7 days.
681
682 Purified HIF complexes bound to carboxyfluorescein (FAM) labeled HRE (IDT) were diluted to
683 a final concentration of 1μM fluorophore, with an addition of 0.05% tween-20. A serial dilution
684 of ligand was generated in ligand buffer (50 mM HEPES (pH 7.4), 50 mM NaCl, 5 mM $MgCl_2$,
685 2-4% DMSO), with concentrations depending on the identity of the ligand. MST samples were
686 generated as a 1:1 (v/v) mix of HIF complex (fixed 500 nM final concentration) to each
687 concentration of the ligand serial dilution. Samples were drawn into standard MST capillaries
688 (NanoTemper) and loaded into a Monolith NT.115 (NanoTemper) for binding analyses. Data
689 were obtained using MO.Control (NanoTemper) and analyzed using PALMIST and GUSSI (59).
690
691 **Cryogenic Electron Microscopy**

692 Purified HIF complexes were concentrated to a final concentration of 10-20 µM (1-2 mg/mL)
693 using 10 kDa Pierce Concentrators (ThermoFisher) at 4°C and 1000xg. TACC3 (residues 788-
694 838) was mixed with the HIF-2 complexes to a final concentration of 70-150 µM and allowed to
695 bind for ~20 min on ice. 3.5 µL of sample was applied to Quantifoil Au 300 R1.2/1.3 with
696 Ultrathin Carbon EM grids (Electron Microscopy Sciences) and plunge frozen using a Vitrobot 3
697 (ThermoFisher) at 100% humidity and 4°C. Frozen grids were then analyzed at the New York
698 Structural Biology Center (NYSBC) Members Electron Microscopy Center (MEMC) using a
699 TFS Titan Krios transmission electron microscope (ThermoFisher). Micrographs were collected
700 at a pixel size of 0.844 Å/px at an exposure rate of 58.94 $e^-/Å^2$/frame with a defocus range of 0.8-
701 2.0 µm. Particles were picked from micrographs and extracted to a box size of 400x400 pixels
702 using Warp (60) and analyzed using CryoSPARC (41). Particles were typically sorted through
703 iterative rounds of 2D classification, *ab initio* reconstruction, and heterogeneous, homogenous
704 and non-uniform refinement.
705
706 **Crystallization and Crystallographic Structure Determination of TACC3(758-838)**
707 12.5 mg/mL of purified human TACC3(758-838) and 9.3 mg/mL of human ARNT PAS-B(356-
708 470) were mixed in 50 mM HEPES, pH 7.4, 50 mM NaCl, 50 mM $MgCl_2$, and 5% glycerol
709 crystallized in 1 M imidazole, pH 7 and 50% (v/v) MPD via the sitting-drop vapor diffusion
710 method. The condition was found via high-throughput screening using NeXtal Protein Complex
711 sparse matrix crystallization screen (NeXtal Technologies; condition H9, the drop contained
712 equal volumes of protein solution and mother liquor). Crystals were harvested directly from the
713 screen and cryoprotected with LV CryoOil (MiTeGen) and flash-cooled in liquid N_2 prior to data
714 collection. Data were collected at the National Synchrotron Light Source II on the AMX (17-ID-

715 1) beamline at Brookhaven National Laboratory. Data were processed using the autoPROC tool
716 box (61) resulting in a 2.28 Å data set. While electron density for ARNT PAS-B was not
717 observed, sufficient density for TACC3 residues 780-836 was visible to allow the structure to be
718 determined by molecular replacement with Phaser (62) using PDB entry 4PKY (chains B and C)
719 as the starting search model. Several cycles of refinement were conducted using Coot (63) and
720 Phenix.refine (64). Data collection, processing and refinement statistics are provided in **Table**
721 **S2**. Coordinates for TACC3(758-838) have been deposited in the RCSB with accession number
722 9OPF, including residues 780-836 on one chain and 782-836 on the other.
723
724 **Structural modeling of HIF complexes**
725 AlphaFold-generated structures were flexibly fit into refined cryo-EM density maps using
726 ChimeraX (65) and ISOLDE (66) to apply distance restraints. For the HIF-2 dimer of
727 heterodimers, we flexibly fit our cryo-EM structure of human HIF-2 into the obtained cryo-EM
728 density. Structures were then further refined using PHENIX (64) to perform global real space
729 refinement and Coot (63) to perform atomic refinement and remove unresolved regions.
730 Structural validation was performed using MolProbity and comprehensive validation in PHENIX
731 (64). For HIF-1 and HIF-2/TACC3 complexes, shTACC3 fragments were fit into corresponding
732 cryo-EM maps (with the HIF complex docked and fixed) using the Dock in Map function of
733 PHENIX (64). Coordinates for HIF-1 and HIF-2 complexes were deposited with RCSB under
734 the following accession numbers: 9OF0 (HIF-2 heterodimer/HRE), 9OF2 (HIF-2 dimer of
735 heterodimers/BS1 HRE+HAS), 9OFU (HIF-1 dimer of heterodimers/BS2 HRE+HAS).
736 Coordinates for models of TACC3/HIF-1/HRE and TACC3/HIF-2/HRE complexes are

737 deposited at PDB-IHM under the accession numbers 4-KM1G (TACC3/HIF-1) and 4-KM1E
738 (TACC3/HIF-2).
739
740 **Size Exclusion Chromatography Coupled with Multi-Angle Light Scattering (SEC-MALS)**
741 Purified HIF complexes were concentrated to a final concentration of 15-20 µM (1-2 mg/mL)
742 using 10 kDa Pierce Concentrators (ThermoFisher) at 4°C and 1000xg. Samples were then
743 filtered through an Ultrafree 0.1 µm centrifugal filter (Millipore) at 4°C and 1000xg. 500 µL of
744 sample were passed through a Superdex 200 10/300 size exclusion column (Cytiva) with the HIF
745 analytical buffer (50 mM HEPES (pH 7.4), 250 mM NaCl, 5 mM $MgCl_2$) before passing through
746 a DAWN HELEOS II MALS detector and an Optilab T-rEX Refractive Index Detector
747 (Wyatt/Waters) using a P-920/UPC-900 AKTA FPLC System (Cytiva). SEC-MALS data was
748 obtained and analyzed using ASTRA (Wyatt/Waters) and plotted in R.
749
750 **Size Exclusion Chromatography for HIF-1/HIF-2 Complex Determination**
751 Human HIF-1α (residues 4-361) and ARNT (residues 91-470) were cloned into a pHis-MBP
752 vector (67) and expressed as detailed above for HIF-complexes. MBP-tagged HIF-1 and HIF-2
753 were separately lysed through sonication and centrifuged for 45 min at 47850xg and 4°C.
754 Lysates were then combined and purified together using an AKTA Püre (Cytiva) by flowing
755 lysate over a 5 mL HisTrap HP (Cytiva), followed by wash buffer (50 mM HEPES, 300 mM
756 NaCl, 20 mM imidazole, 2 mM BME) with stepwise increasing concentrations of imidazole (20
757 mM, 68 mM, 164 mM, 260 mM) to remove nonspecifically bound protein. Mixed proteins were
758 then eluted with elution buffer (50 mM HEPES (pH 7.4), 300 mM NaCl, 500 mM imidazole, 2
759 mM BME), then mixed with about a 20x molar excess of 51 bp BS1 HRE, 51 bp BS1 HRE with

760 a mutated HRE-box, or 51 bp BS1 HRE with a mutated HAS-box (IDT) and 5 mM $MgCl_2$ and
761 allowed to bind at 4°C overnight (10-16 hr). Protein was then concentrated about 10x by
762 dialyzing (3.5 kDa MWCO dialysis tubing, ThermoFisher) against dry polyethylene glycol
763 35000. DNA-bound MBP-HIF-1/HIF-2 complexes were further purified through a Superdex 200
764 increase 16/40 HiScale (Cytiva) with the final analytical buffer (50 mM HEPES, (pH 7.4) 250
765 mM NaCl, 5 mM $MgCl_2$) to separate complexes via size exclusion chromatography. Complex
766 components were then visualized using gel electrophoresis. SEC profiles were plotted in R.
767
768 Mutant HRE-box BS1 HRE+HAS:
769 AGGGGTGGAGGGGGCTGttaaaTgatatCTGTCTCACACAGCCTGTCTGAC
770 Mutant HAS-box BS1 HRE+HAS:
771 AGGGGTGGAGGGGGCTGGGCCCTACGTGCTGTCgatatgtcgaCtTCTGAC
772
773 **Hydrogen Deuterium Exchange Coupled with Mass Spectrometry (HDX-MS)**
774 Purified 20 bp HRE-bound HIF-2 was incubated with shTACC3 for one hour in about a 3:1
775 molar ratio of TACC3 to HIF-2 (74 μM shTACC3 and 24 μM HIF-2) or an equivalent volume of
776 TACC3 buffer (50 mM HEPES, 50 mM NaCl, 5 mM $MgCl_2$). Using a LEAP HDX Automation
777 Platform (Trajan Automation), the protein mixture was deuterated in D_2O buffer (50 mM
778 HEPES, 50 mM NaCl, 5 mM $MgCl_2$, solvated in 100% D_2O) for varying timepoints (0 s, 50 s,
779 300 s, 1000 s, 3000 s, 5000 s) after which the deuterated protein mixture was mixed with quench
780 buffer (3 M guanidinium HCl, 3% acetonitrile, 1% formic acid) at 0°C. Samples were then
781 loaded onto a Waters Enzymate BEH Pepsin Column for proteolysis followed by a C18
782 analytical column (Hypersil Gold, 50 mm length × 1 mm diameter, 1.9 μm particle size,

783 ThermoFisher Scientific) before being loaded onto a maXis-II ETD ESI-qTOF mass
784 spectrometer (Bruker) for fragment mass analysis. Timepoints both with and without TACC3
785 present were completed in triplicate. Raw HDX data was analyzed using Bruker Compass Data
786 Analysis 5.3 and Biotools 3.2 software and further analyzed with HDexaminer (Sierra
787 Analytics/Trajan Automation) to calculate relative exchange rates before being plotted in R.
788

789 **Reporter assays**

790 Luciferase reporter assays were performed with transiently transfected HEK293T cells. Cells
791 were plated onto 48-well plates at 100,000 cells/well. Twenty-four hours later, cells were
792 transfected in triplicate with Lipofectamine 2000 (Invitrogen). Each well received 33 ng reporter
793 plasmid under control of wild-type or mutant human 3' erythropoietin (Epo) enhancer fused to a
794 firefly luciferase cassette (pGL3-Basic, Promega), 200 ng empty expression plasmid (pIRES-
795 hrGFP-2a, Stratagene), and 100 ng plasmid expressing oxygen insensitive "PPN" HIF-1α or
796 HIF-2α variants, which contain mutations in two proline and one asparagine residue that are
797 normally subject to O_2-dependent post-translational modifications (68). At 24 hr post-
798 transfection, cells were rinsed one time with PBS (ThermoFisher), followed by lysis with 50 μL
799 core luciferase buffer (30 mM tricine (pH 7.8), 8 mM magnesium acetate, 0.2 mM EDTA, 1%
800 Triton X-100, and 100 mM 2-mercaptoethanol). Luciferase assays were performed by adding 50
801 μL substrate buffer (core buffer supplemented with 2.5 mM $MgCl_2$, 1.5 mM ATP, 0.5 mM
802 coenzyme A, and 0.5 mM D-luciferin) to 10 μL cell lysate and immediately reading
803 luminescence on a CLARIOstar Plus plate reader (BMG Labtech). Long oligos with Nhe I and
804 Xho I restriction sites at the 5' and 3' ends, respectively, were used to position the 3' human Epo

805 enhancer upstream of a minimal mouse Epo promoter. Sequences of the 3' human Epo enhancer
806 sequences used in this study are indicated below (mutations and restriction sites in lowercase):
807
808 <u>WT:</u>
809 gctagcAGATCTGGGAAACGAGGGGTGGAGGGGGCTGGGCCCTACGTGCTGTCTCACA
810 CAGCCTGTCTGACCTCTCGACCCTACCGGGCCTGAGGCCACAAGCTCTGCCTACGCT
811 GGTCAATAAGGTGGCTCCATTCAAGGCCTCACCGCAGTAAGGCAGCTGCCAACCCTc
812 gag
813
814 <u>GC-rich mutant:</u>
815 gctagcAGATCTGGGAAACGAGGctaGaAttcctCTGGGCCCTACGTGCTGTCTCACACAGCC
816 TGTCTGACCTCTCGACCCTACCGGGCCTGAGGCCACAAGCTCTGCCTACGCTGGTCA
817 ATAAGGTGGCTCCATTCAAGGCCTCACCGCAGTAAGGCAGCTGCCAACCCTcgag
818
819 <u>HRE mutant:</u>
820 gctagcAGATCTGGGAAACGAGGGGTGGAGGGGGCTGttaaaTgatatCTGTCTCACACAGCC
821 TGTCTGACCTCTCGACCCTACCGGGCCTGAGGCCACAAGCTCTGCCTACGCTGGTCA
822 ATAAGGTGGCTCCATTCAAGGCCTCACCGCAGTAAGGCAGCTGCCAACCCTcgag
823
824 <u>HAS mutant:</u>
825 gctagcAGATCTGGGAAACGAGGGGTGGAGGGGGCTGGGCCCTACGTGCTGTCgatatgtcg
826 aCtTCTGACCTCTCGACCCTACCGGGCCTGAGGCCACAAGCTCTGCCTACGCTGGTCA
827 ATAAGGTGGCTCCATTCAAGGCCTCACCGCAGTAAGGCAGCTGCCAACCCTcgag

828

829 **Acknowledgements**

830 We thank Dan Lee and Julia Simon for technical assistance, Soumendu Boral and other members
831 of the Gardner laboratory as well as Rick Bruick, Uttam Tambar, Qing Zhang, and Derek Tan for
832 helpful discussions. This work was supported by NIH grants U54 CA132378 and U54
833 CA137788 (to K.H.G.), Mathers Foundation grant MF-2112-02288 (to K.H.G. and J.A.G.), and
834 funds from the Department of Veterans Affairs I01BX000446 (to J.A.G.). Cryo-EM data
835 collection was performed at the Members Electron Microscopy Center at the New York
836 Structural Biology Center, with major support from the Simons Foundation (SF349247). This
837 research used the AMX and FMX beamlines of the National Synchrotron Light Source II, a U.S.
838 Department of Energy (DOE) Office of Science User Facility operated for the DOE Office of
839 Science by Brookhaven National Laboratory under Contract No. DE-SC0012704.

840

841 **Figure Legends**

842 **Figure 1. Schematic of HIF pathway regulation and components.** (A) Under normoxic
843 conditions, HIF-α is inactivated in the cytosol through parallel oxygen-dependent post-
844 translational hydroxylations of residues in the protein C-terminus. These include a proline-
845 directed mechanism (HIF-1α: Pro402 and 562, HIF-2α: Pro405 and 531) which leads to the
846 recruitment of the von Hippel-Lindau E3 ubiquitin ligase, leading to poly-ubiquitination and
847 proteosomal degradation (3, 4). A second route focuses on an asparagine residue (HIF-1α:
848 Asn803, HIF-2α: Asn851) in the C-terminal transactivation domain (CTAD), preventing
849 recruitment of CBP/p300 coactivators essential for HIF-driven transcriptional activation (5, 6).
850 Under hypoxic conditions, neither of these HIF-α hydroxylations occur, allowing the fully
851 functional protein to accumulate, translocate into to the nucleus, and heterodimerizes with
852 ARNT. The HIF-α-ARNT complex then associates with specific HRE sequences in the promoter
853 or enhancer regions of oxygen-dependent genes and recruits coactivators, leading to
854 transcriptional activation. (B) Schematic depicting the domain arrangements of human HIF-2α
855 and ARNT, as well as indicating which domains interact with HRE DNA as well as CCC- and
856 CBP/p300-type transcriptional coactivators.
857

858 **Figure 2. Cryo-EM structural analysis of human HIF-2 bound to 20 bp HRE fragments.**
859 (A) Cryo-EM 2D classes of HIF-2 complexes, with individual PAS and bHLH domains and
860 DNA visible. (B) Some 2D classes of HIF-2 complexes showed either an apparent ARNT PAS-
861 B detached from the rest of the HIF-2a-ARNT core (left) or destabilized bHLH domains lacking
862 bound DNA (right). (C) 3.61 Å EM map (262,466 particles, 13.3% of all collected particles) was
863 generated from refinement of the most populated *ab initio* volume into which an AlphaFold 2
864 model of human HIF-2 was fit. (D) Overlay of the mouse HIF-2 crystal structure (PDB code:
865 4ZPK, (9)) and human HIF-2 cryo-EM structure show highly similar domain architectures. (E)
866 Local resolutions mapped onto the HIF-2 cryo-EM density map show a region of particularly
867 low local resolution/high flexibility in the ARNT PAS-B (Fα-helix, Gβ-strand, Hβ strand)
868 domain and bHLH domains.
869
870 **Figure 3. Structural and biochemical analyses of HIF dimer-of-heterodimer complexes.** (A)
871 2D cryo-EM class averages from analyses of data collected on HIF-2α-ARNT heterodimers
872 bound to 51 bp BS1 HRE/HAS DNA fragments, showing markedly different (and often, more
873 symmetrical) arrangements than comparable 2D class averages of HIF-2 bound to 20 bp HRE
874 DNAs. (B) A 3.74 Å EM map (164,352 particles, 25.0% of all collected particles) was generated
875 from refinement of the most populated *ab initio* volume into which two individually assembled
876 human HIF-2 heterodimers were fit, along with the corresponding 51 bp BS1 HRE/HAS DNA
877 fragment. (C) Local resolution data mapped onto the HIF-2 dimer-of-heterodimers cryo-EM map
878 showed that the ARNT PAS-B Fα-helix and Gβ-strand were higher relative resolution than in
879 corresponding sections of the 20 bp HRE-bound HIF-2 EM map, suggestive of ordering between
880 the heterodimer and dimer-of-heterodimer complexes. (D) The 3.90 Å cryo-EM map (71,802
881 particles, 27.3% of all collected particles) of HIF-1 bound to a 52 bp BS2 HRE/HAS DNA
882 fragment showed a highly similar domain arrangement to HIF-2, though the ARNT PAS-A
883 domains were less resolved. (E) Highlighted residues were suspected to form interactions
884 between the opposing ARNT PAS-B domains in the HIF-2 supercomplex (basic residues in blue,
885 acidic residues in red, uncharged residues in magenta) (F) SEC-MALS data showed expected
886 differences in the molecular weights of HIF-2 on 20 bp HRE DNA fragments (96.7±6.3 kDa)
887 and 51 bp BS1 HRE/HAS DNA fragments (214.0±14.1 kDa), but revealed an intermediate value
888 (144.0±6.9 kDa) for a HIF-2 variant with mutations in four key ARNT PAS-B Fα-helix and Gβ-
889 strand residues which are at the ARNT/ARNT interface essential to the dimer-of-heterodimers
890 complex. (G) Luciferase reporter assays containing the wildtype (WT) or mutant versions of the
891 human EPO enhancer with changes in the upstream GC-rich region (GC-rich-mut), HRE (HRE-
892 mut), or HAS (HAS-mut) site were performed in HEK293T cells in conjunction with ectopic
893 expression of oxygen-independent (PPN) HIF-1α or HIF-2α. Empty pIRES vector expression
894 was measured to ensure empty vector would not contribute to reporter response. Mutations to
895 either the HRE or HAS site substantially blunted reporter induction by either PPN HIF-1α and
896 PPN HIF-2α.
897

898 **Figure 4. Contextual differences impact small molecule binding to ARNT and HIF-a PAS-**
899 **B domains.** (A) Known small molecule binders of isolated ARNT (KG-548 (1, 2), KG-279 (1,
900 2)) and HIF-2a PAS-B (compound 2 (7), PT2385 (8)) domains are shown along with their
901 literature affinities for the specific PAS-B targets, obtained by microscale thermophoresis, ITC,
902 and NMR. (B) Inclusion of the ARNT and HIF-2a PAS-B domains within a DNA-bound HIF-2
903 heterodimer substantially modulates binding affinities of PAS-B binding compounds compared
904 to the free PAS-B domains, as assayed by MST with a fluorescein label attached to the 5' end of
905 one strand of a 20 bp HRE duplex. (C) Incorporation of the PAS-B domains within a DNA-
906 bound HIF-2 dimer of heterodimers further changes PAS-B ligand binding affinities, as detected
907 with fluorescein label attached to the 5' end of one strand of a 51 bp BS1 HRE/HAS duplex.
908
909 **Figure 5. Coiled-coil coactivator binding to HIF heterodimers.** (A, B) MST measurements of
910 C-terminal fragments of CoCoA(407-535) and TACC3(758-838) binding to the (A) isolated
911 ARNT PAS-B domains and (B) HIF-2α-ARNT heterodimers (HIF-2) bound to 20 bp HRE
912 fragments. The two highest points of the hCoCoA to HIF-2 binding curve showed evidence of
913 aggregation and were removed. TACC3 binding to HIF-2 showed a decrease at high
914 concentration, suggesting a second binding mode or aggregation. (C) A truncated TACC3(788-
915 838, "shTACC3") was designed based on our TACC3(758-838) crystal structure showing highly
916 elevated B-factors and poor electron density in residues 758-788. This CCC fragment bound a 20
917 bp HRE-bound HIF-2 with a minimal affinity drop from the longer TACC3 (K_d 26 μM by MST),
918 and without the secondary binding mode seen for longer fragments to HIF-2. (D) 2D classes of
919 shTACC3 bound to 20 bp HRE-bound HIF-2 showed visible core domains with excess blurred
920 density extending out of the central region. (E) *Ab initio* reconstruction of 20 bp HRE-bound
921 HIF-2 bound to shTACC3. HIF-2 fit into the volume without major rearrangement, leaving
922 excess density along the ARNT PAS-B/HIF-2α PAS-A interface for most of shTACC3 to be fit.
923 (F) Schematic of interactions between TACC3(788-838) and HIF-2 shows three PAS domains
924 interacting with the TACC3 coiled coil. Residues indicated on TACC3 originate from either
925 chain. (G) Cryo-EM of HIF-1 bound to the longer TACC3(758-858) fragment showed similar
926 excess density as HIF-2/TACC3(788-838), consistent with TACC3 binding similarly to HIF-1
927 and HIF-2. TACC3 residues 793-838 were confidently fit into the excess density for both HIF-1
928 and HIF-2. (H) HDX-MS deuterium uptake plots showed several HIF-2α and ARNT loops with
929 increased protection from solvent in the presence of TACC3. (I) Mapping peptides with TACC3-
930 induced HDX changes onto shTACC3-bound HIF-2 model (increased protection in green)
931 showed these protected loops along the proposed TACC3 binding interface from cryo-EM.
932
933 **Figure 6. Proposed promoter-dependent formation of higher-order HIF and their**
934 **downstream effects.** (A) Under hypoxic conditions, we propose HIFs form different complexes
935 based on the sequence of the promoter/enhancer region of the gene of interest. For HRE-only
936 containing genes, we propose HIFs form a single heterodimer on the HRE-box, recruiting other
937 components such as CCCs. For genes containing an HRE-box followed by an 8 bp spacer and an

938 HAS-box, we propose that HIFs instead form a dimer-of-heterodimers. We suggest the
939 specification of which genes are activated by HIF are dose dependent, in that lower cellular
940 levels of HIF will activate HRE-only genes while higher cellular levels of HIF will activate
941 HRE/HAS containing genes. Additionally, HIF-α can form noncanonical complexes with
942 alternative class II bHLH-PAS proteins, including BMAL1, as well as mixed HIF-1/HIF-2
943 dimer-of-heterodimer complexes, each under varying conditions. We suggest that the similar
944 quaternary structure of the HIF-2α-BMAL1 complex lends itself to the potential formation of
945 dimer-of-heterodimers structures, though this remains to be experimentally validated.
946

947 **References**

948 1. X. Xu *et al.*, Identification of Small Molecule Ligand Binding Sites On and In the ARNT PAS-B
949 Domain. *Journal of Biological Chemistry* **300**, 107606 (2024).
950 2. Y. Guo *et al.*, Regulating the ARNT/TACC3 axis: Multiple approaches to manipulating
951 protein/protein interactions with small molecules. *ACS chemical biology* **8**, 626-635 (2013).
952 3. G. L. Semenza, Hypoxia-inducible factor 1 (HIF-1) pathway. *Science's STKE: signal*
953 *transduction knowledge environment* **2007**, cm8 (2007).
954 4. M. Strowitzki, E. Cummins, C. Taylor, Protein Hydroxylation by Hypoxia-Inducible Factor (HIF)
955 Hydroxylases: Unique or Ubiquitous? *Cells* **8**, 384 (2019).
956 5. D. Lando *et al.*, FIH-1 is an asparaginyl hydroxylase enzyme that regulates the transcriptional
957 activity of hypoxia-inducible factor. *Genes & Development* **16**, 1466-1471 (2002).
958 6. D. Lando, D. J. Peet, D. A. Whelan, J. J. Gorman, M. L. Whitelaw, Asparagine Hydroxylation of
959 the HIF Transactivation Domain: A Hypoxic Switch. *Science* **295**, 858-861 (2002).
960 7. T. H. Scheuermann *et al.*, Allosteric Inhibition of Hypoxia Inducible Factor-2 with Small
961 Molecules. *Nature chemical biology* **9**, 271-276 (2013).
962 8. P. M. Wehn *et al.*, Design and Activity of Specific Hypoxia-Inducible Factor-2α (HIF-2α)
963 Inhibitors for the Treatment of Clear Cell Renal Cell Carcinoma: Discovery of Clinical Candidate
964 (S)-3-((2,2-Difluoro-1-hydroxy-7-(methylsulfonyl)-2,3-dihydro-1H-inden-4-yl)oxy)-5-
965 fluorobenzonitrile (PT2385). *Journal of Medicinal Chemistry* **61**, 9691-9721 (2018).
966 9. D. Wu, N. Potluri, J. Lu, Y. Kim, F. Rastinejad, Structural integration in hypoxia-inducible
967 factors. *Nature* **524**, 303-308 (2015).
968 10. D. C. Bersten, A. E. Sullivan, D. J. Peet, M. L. Whitelaw, bHLH-PAS proteins in cancer. *Nature*
969 *Reviews. Cancer* **13**, 827-841 (2013).
970 11. N. Albadari, S. Deng, W. Li, The transcriptional factors HIF-1 and HIF-2 and their novel
971 inhibitors in cancer therapy. *Expert Opinion on Drug Discovery* **14**, 667-682 (2019).
972 12. S. Kaluz, M. Kaluzová, E. J. Stanbridge, Regulation of gene expression by hypoxia: integration
973 of the HIF-transduced hypoxic signal at the hypoxia-responsive element. *Clinica chimica acta;*
974 *international journal of clinical chemistry* **395**, 6-13 (2008).
975 13. T. Rosell-Garcia *et al.*, Multimerization of HIF enhances transcription of target genes containing
976 the hypoxia ancillary sequence. *Biochimica et Biophysica Acta (BBA) - Gene Regulatory*
977 *Mechanisms* **1866**, 194963 (2023).
978 14. C. L. Partch, K. H. Gardner, Coactivators necessary for transcriptional output of the hypoxia
979 inducible factor, HIF, are directly recruited by ARNT PAS-B. *Proceedings of the National*
980 *Academy of Sciences* **108**, 7739-7744 (2011).
981 15. Y. Guo, T. H. Scheuermann, C. L. Partch, D. R. Tomchick, K. H. Gardner, Coiled-coil
982 Coactivators Play a Structural Role Mediating Interactions in Hypoxia-inducible Factor
983 Heterodimerization. *The Journal of Biological Chemistry* **290**, 7707-7721 (2015).
984 16. J. C. Jun, A. Rathore, H. Younas, D. Gilkes, V. Y. Polotsky, Hypoxia-Inducible Factors and
985 Cancer. *Current sleep medicine reports* **3**, 1-10 (2017).
986 17. S. Mazumder, P. J. Higgins, R. Samarakoon, Downstream Targets of VHL/HIF-α Signaling in
987 Renal Clear Cell Carcinoma Progression: Mechanisms and Therapeutic Relevance. *Cancers* **15**,
988 1316 (2023).
989 18. E. E. Wicks, G. L. Semenza, Hypoxia-inducible factors: cancer progression and clinical
990 translation. *The Journal of Clinical Investigation* **132**, e159839.
991 19. C.-J. Hu, L.-Y. Wang, L. A. Chodosh, B. Keith, M. C. Simon, Differential roles of hypoxia-
992 inducible factor 1alpha (HIF-1alpha) and HIF-2alpha in hypoxic gene regulation. *Molecular and*
993 *Cellular Biology* **23**, 9361-9374 (2003).
994 20. E. B. Rankin *et al.*, Hypoxia-inducible factor–2 (HIF-2) regulates hepatic erythropoietin in vivo.
995 *The Journal of Clinical Investigation* **117**, 1068-1077 (2007).

21. S. Hara, J. Hamada, C. Kobayashi, Y. Kondo, N. Imura, Expression and Characterization of Hypoxia-Inducible Factor (HIF)-3α in Human Kidney: Suppression of HIF-Mediated Gene Expression by HIF-3α. *Biochemical and Biophysical Research Communications* **287**, 808-813 (2001).
22. A. M. Fala *et al.*, Unsaturated fatty acids as high-affinity ligands of the C-terminal Per-ARNT-Sim domain from the Hypoxia-inducible factor 3α. *Scientific Reports* **5**, 12698 (2015).
23. Z.-j. Liu, G. L. Semenza, H.-f. Zhang, Hypoxia-inducible factor 1 and breast cancer metastasis. *Journal of Zhejiang University. Science. B* **16**, 32-43 (2015).
24. D. Wu *et al.*, Bidirectional Modulation of HIF-2 Activity through Chemical Ligands. *Nature chemical biology* **15**, 367-376 (2019).
25. E. Jonasch *et al.*, Belzutifan for Renal Cell Carcinoma in von Hippel–Lindau Disease. *New England Journal of Medicine* **385**, 2036-2046 (2021).
26. T. K. Choueiri *et al.*, Inhibition of hypoxia-inducible factor-2α in renal cell carcinoma with belzutifan: a phase 1 trial and biomarker analysis. *Nature medicine* **27**, 802-805 (2021).
27. X. Diao *et al.*, Identification of oleoylethanolamide as an endogenous ligand for HIF-3α. *Nature Communications* **13**, 2529 (2022).
28. W. Ruan *et al.*, BMAL1–HIF2A heterodimer modulates circadian variations of myocardial injury. *Nature* **641**, 1017-1028 (2025).
29. N. Huang *et al.*, Crystal Structure of the Heterodimeric CLOCK:BMAL1 Transcriptional Activator Complex. *Science (New York, N.Y.)* **337**, 189-194 (2012).
30. G. L. Semenza, G. L. Wang, A nuclear factor induced by hypoxia via de novo protein synthesis binds to the human erythropoietin gene enhancer at a site required for transcriptional activation. *Molecular and Cellular Biology* **12**, 5447-5454 (1992).
31. B. L. Ebert, H. F. Bunn, Regulation of Transcription by Hypoxia Requires a Multiprotein Complex That Includes Hypoxia-Inducible Factor 1, an Adjacent Transcription Factor, and p300/CREB Binding Protein. *Molecular and Cellular Biology* **18**, 4089-4096 (1998).
32. H. Kimura *et al.*, Identification of Hypoxia-inducible Factor 1 Ancillary Sequence and Its Function in Vascular Endothelial Growth Factor Gene Induction by Hypoxia and Nitric Oxide *. *Journal of Biological Chemistry* **276**, 2292-2298 (2001).
33. F. Corrêa, J. Key, B. Kuhlman, K. H. Gardner, Computational Repacking of HIF-2α Cavity Replaces Water-Based Stabilized Core. *Structure* **24**, 1918-1927 (2016).
34. X. Ren, X. Diao, J. Zhuang, D. Wu, Structural basis for the allosteric inhibition of hypoxia-inducible factor (HIF)-2 by belzutifan. *Molecular Pharmacology* 10.1124/molpharm.122.000525, MOLPHARM-AR-2022-000525 (2022).
35. T. H. Scheuermann *et al.*, Artificial ligand binding within the HIF2α PAS-B domain of the HIF2 transcription factor. *Proceedings of the National Academy of Sciences* **106**, 450-455 (2009).
36. S. A. Dames, M. Martinez-Yamout, R. N. De Guzman, H. J. Dyson, P. E. Wright, Structural basis for Hif-1α/CBP recognition in the cellular hypoxic response. *Proceedings of the National Academy of Sciences* **99**, 5271-5276 (2002).
37. T. V. Beischlag *et al.*, Recruitment of Thyroid Hormone Receptor/Retinoblastoma-interacting Protein 230 by the Aryl Hydrocarbon Receptor Nuclear Translocator Is Required for the Transcriptional Response to Both Dioxin and Hypoxia *. *Journal of Biological Chemistry* **279**, 54620-54628 (2004).
38. M. P. Labrecque *et al.*, A TRIP230-Retinoblastoma Protein Complex Regulates Hypoxia-Inducible Factor-1α-Mediated Transcription and Cancer Cell Invasion. *PLOS ONE* **9**, e99214 (2014).
39. C. L. Partch, P. B. Card, C. A. Amezcua, K. H. Gardner, Molecular Basis of Coiled Coil Coactivator Recruitment by the Aryl Hydrocarbon Receptor Nuclear Translocator (ARNT)*. *Journal of Biological Chemistry* **284**, 15184-15192 (2009).
40. J. H. Kim, M. R. Stallcup, Role of the Coiled-coil Coactivator (CoCoA) in Aryl Hydrocarbon Receptor-mediated Transcription*. *Journal of Biological Chemistry* **279**, 49842-49848 (2004).

41. A. Punjani, J. L. Rubinstein, D. J. Fleet, M. A. Brubaker, cryoSPARC: algorithms for rapid unsupervised cryo-EM structure determination. *Nature Methods* **14**, 290-296 (2017).
42. A. Punjani, H. Zhang, D. J. Fleet, Non-uniform refinement: adaptive regularization improves single-particle cryo-EM reconstruction. *Nature Methods* **17**, 1214-1221 (2020).
43. H. R. López-Mirabal, J. R. Winther, Redox characteristics of the eukaryotic cytosol. *Biochimica Et Biophysica Acta* **1783**, 629-640 (2008).
44. V. L. Dengler, M. Galbraith, J. M. Espinosa, Transcriptional Regulation by Hypoxia Inducible Factors. *Critical reviews in biochemistry and molecular biology* **49**, 1-15 (2014).
45. D. Gagné *et al.*, Use of High Pressure NMR Spectroscopy to Rapidly Identify Proteins with Internal Ligand-Binding Voids. 10.1101/2020.08.25.267195 (2023).
46. G. L. Wang, G. L. Semenza, General involvement of hypoxia-inducible factor 1 in transcriptional response to hypoxia. *Proceedings of the National Academy of Sciences* **90**, 4304-4308 (1993).
47. J. Contenti *et al.*, HIF-1 inactivation empowers HIF-2 to drive hypoxia adaptation in aggressive forms of medulloblastoma. *Cell Death Discovery* **10** (2024).
48. M. Y. Koh, G. Powis, Passing the baton: the HIF switch. *Trends in Biochemical Sciences* **37**, 364-372 (2012).
49. R. M. Mello *et al.* (2024) BMAL1-HIF2α heterodimers contribute to ccRCC. (Cold Spring Harbor Laboratory).
50. A. K. Michael *et al.*, Cooperation between bHLH transcription factors and histones for DNA access. *Nature* **619**, 385-393 (2023).
51. D. Wu, X. Su, N. Potluri, Y. Kim, F. Rastinejad, NPAS1-ARNT and NPAS3-ARNT crystal structures implicate the bHLH-PAS family as multi-ligand binding transcription factors. *eLife* **5**, e18790.
52. X. Diao *et al.*, Structural basis for the ligand-dependent activation of heterodimeric AHR-ARNT complex. *Nature Communications* **16** (2025).
53. J. H. Kim, H. Li, M. R. Stallcup, CoCoA, a Nuclear Receptor Coactivator which Acts through an N-Terminal Activation Domain of p160 Coactivators. *Molecular Cell* **12**, 1537-1549 (2003).
54. J. H. Kim, C. K. Yang, M. R. Stallcup, Downstream signaling mechanism of the C-terminal activation domain of transcriptional coactivator CoCoA. *Nucleic Acids Research* **34**, 2736-2750 (2006).
55. J. H. Nahm *et al.*, Transforming acidic coiled-coil-containing protein 3 (TACC3) overexpression in hepatocellular carcinomas is associated with "stemness" and epithelial-mesenchymal transition-related marker expression and a poor prognosis. *Tumour Biology: The Journal of the International Society for Oncodevelopmental Biology and Medicine* **37**, 393-403 (2016).
56. Y.-L. Wen *et al.*, Transforming acidic coiled-coil protein-3: a novel marker for differential diagnosis and prognosis prediction in endocervical adenocarcinoma. *Molecular Medicine* **27**, 60 (2021).
57. C. L. Partch, K. H. Gardner, Coactivator recruitment: A new role for PAS domains in transcriptional regulation by the bHLH-PAS family. *Journal of Cellular Physiology* **223**, 553-557 (2010).
58. R. Missiaen, N. P. Lesner, M. C. Simon, HIF: a master regulator of nutrient availability and metabolic cross-talk in the tumor microenvironment. *The EMBO Journal* **42** (2023).
59. T. H. Scheuermann, S. B. Padrick, K. H. Gardner, C. A. Brautigam, On the acquisition and analysis of microscale thermophoresis data. *Analytical Biochemistry* **496**, 79-93 (2016).
60. D. Tegunov, P. Cramer, Real-time cryo-electron microscopy data preprocessing with Warp. *Nature Methods* **16**, 1146-1152 (2019).
61. C. Vonrhein *et al.*, Data processing and analysis with the autoPROC toolbox. *Acta Crystallographica Section D Biological Crystallography* **67**, 293-302 (2011).
62. A. J. McCoy *et al.*, Phaser crystallographic software. *Journal of Applied Crystallography* **40**, 658-674 (2007).

1097 63. P. Emsley, B. Lohkamp, W. G. Scott, K. Cowtan, Features and development of Coot. *Acta*
1098 *Crystallographica. Section D, Biological Crystallography* **66**, 486-501 (2010).
1099 64. D. Liebschner *et al.*, Macromolecular structure determination using X-rays, neutrons and
1100 electrons: recent developments in Phenix. *Acta Crystallographica Section D: Structural Biology*
1101 **75**, 861-877 (2019).
1102 65. E. C. Meng *et al.*, UCSF ChimeraX: Tools for structure building and analysis. *Protein Science*
1103 **32**, e4792 (2023).
1104 66. T. I. Croll, ISOLDE: a physically realistic environment for model building into low-resolution
1105 electron-density maps. *Acta Crystallographica Section D: Structural Biology* **74**, 519-530 (2018).
1106 67. P. Sheffield, S. Garrard, Z. Derewenda, Overcoming Expression and Purification Problems of
1107 RhoGDI Using a Family of "Parallel" Expression Vectors. *Protein Expression and Purification*
1108 **15**, 34-39 (1999).
1109 68. E. M. Dioum *et al.*, Regulation of Hypoxia-Inducible Factor 2α Signaling by the Stress-
1110 Responsive Deacetylase Sirtuin 1. *Science* **324**, 1289-1293 (2009).
1111

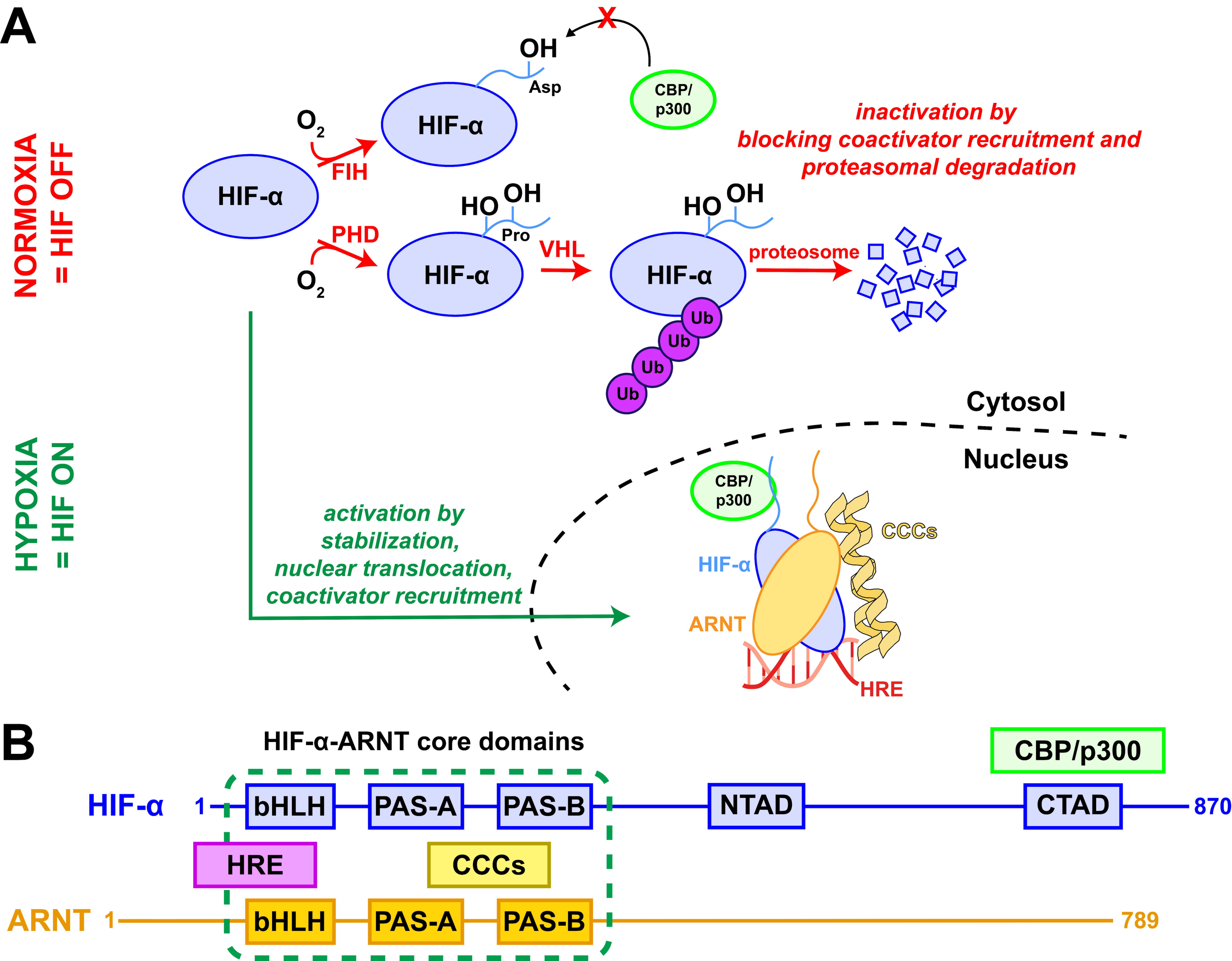
A
NORMOXIA
= HIF OFF
HYPOXIA
= HIF ON
HIF-α
O2
FIH
OH
Asp
X
CBP/
p300
inactivation by
blocking coactivator recruitment and
proteasomal degradation
PHD
HO
OH
Pro
VHL
proteosome
Ub
Cytosol
Nucleus
activation by
stabilization,
nuclear translocation,
coactivator recruitment
CCCs
ARNT
HRE
B
HIF-α-ARNT core domains
CBP/p300
HIF-α
1
bHLH
PAS-A
PAS-B
NTAD
CTAD
870
HRE
CCCs
ARNT
789

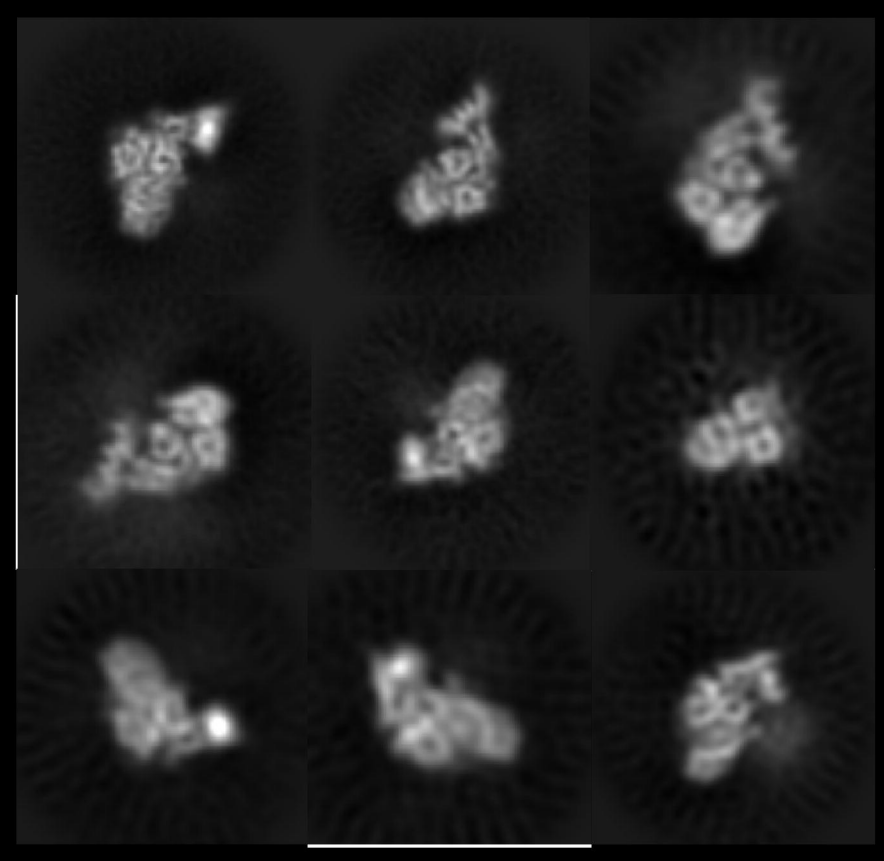

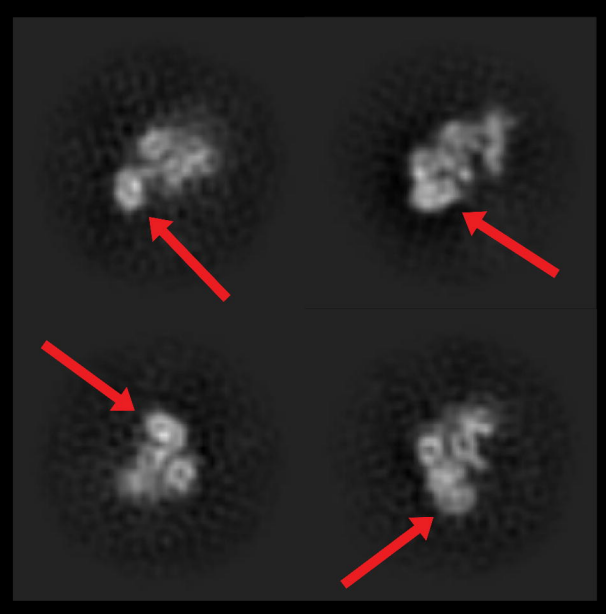

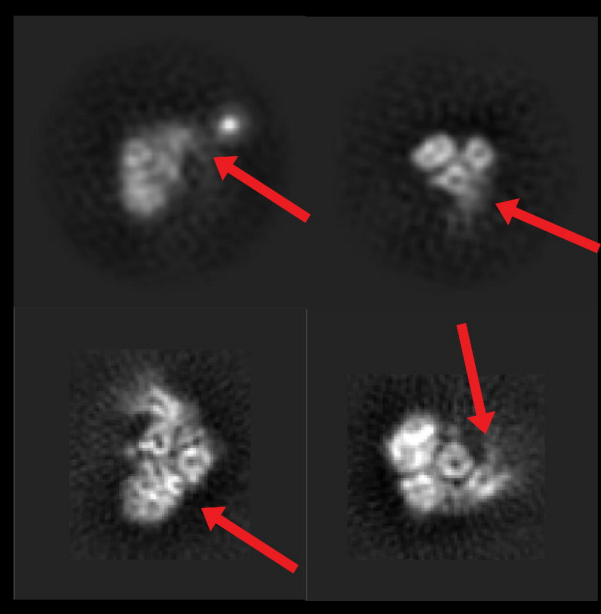

HIF-2α ARNT 20-bp HRE

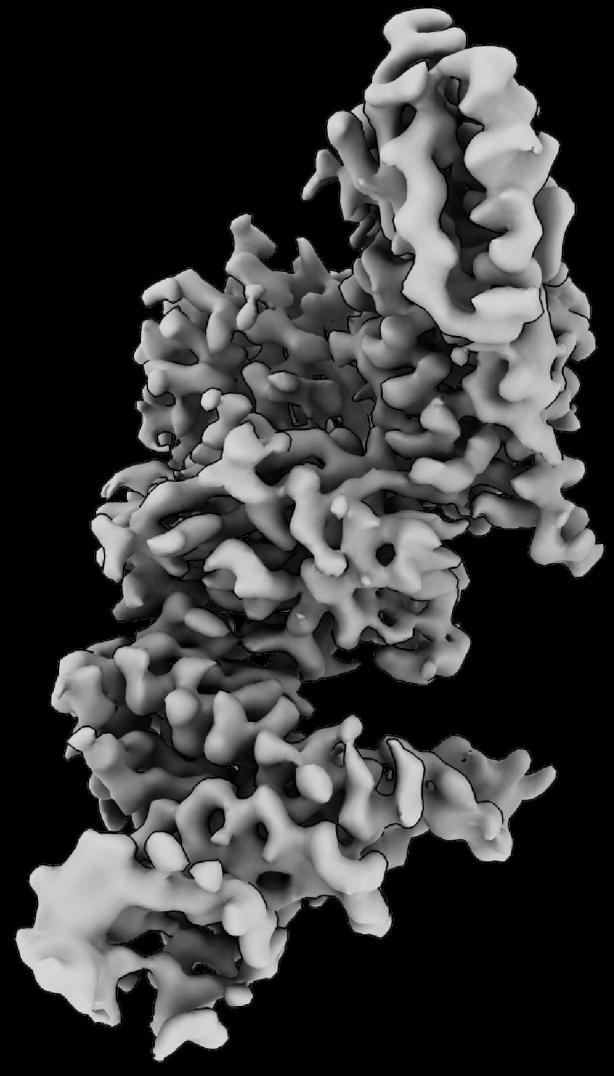

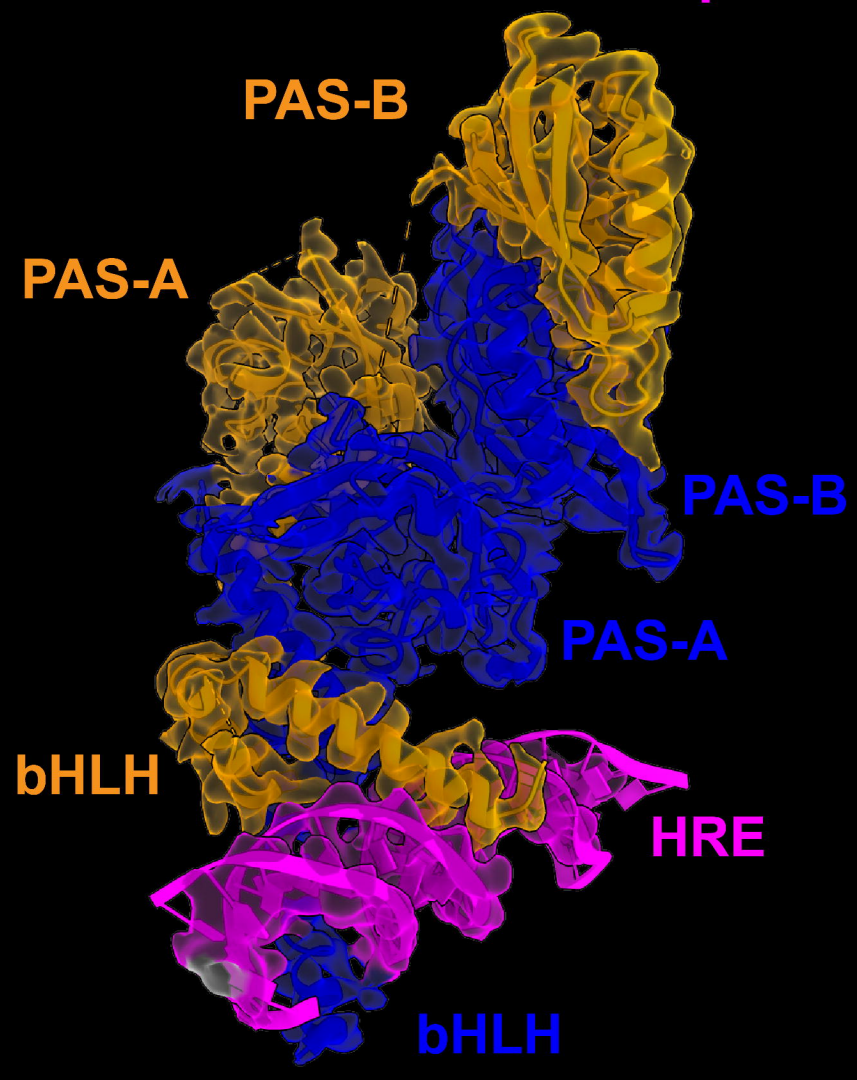

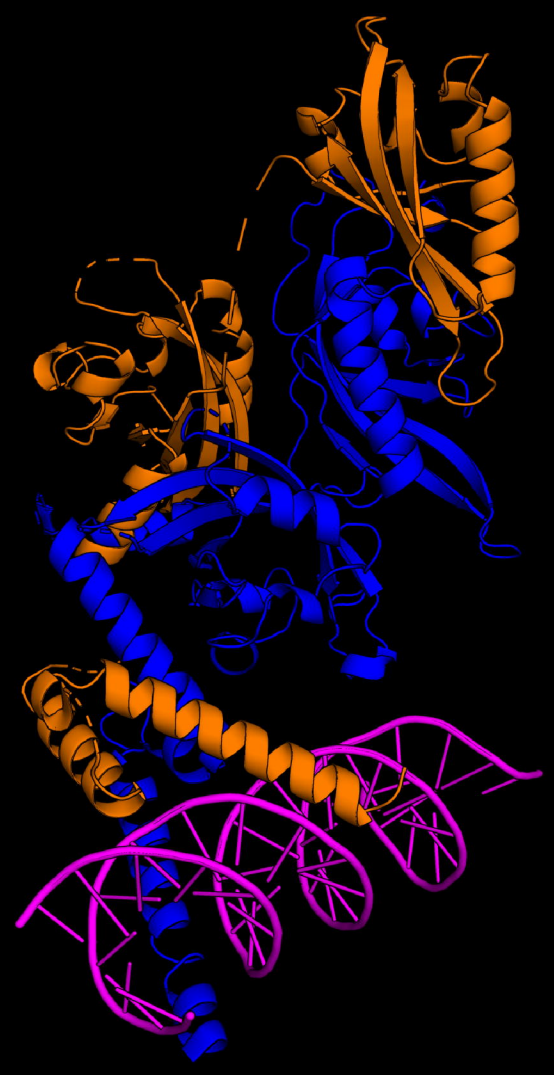

HIF-2α ARNT
20-bp HRE

HIF-2α ARNT
20-bp HRE

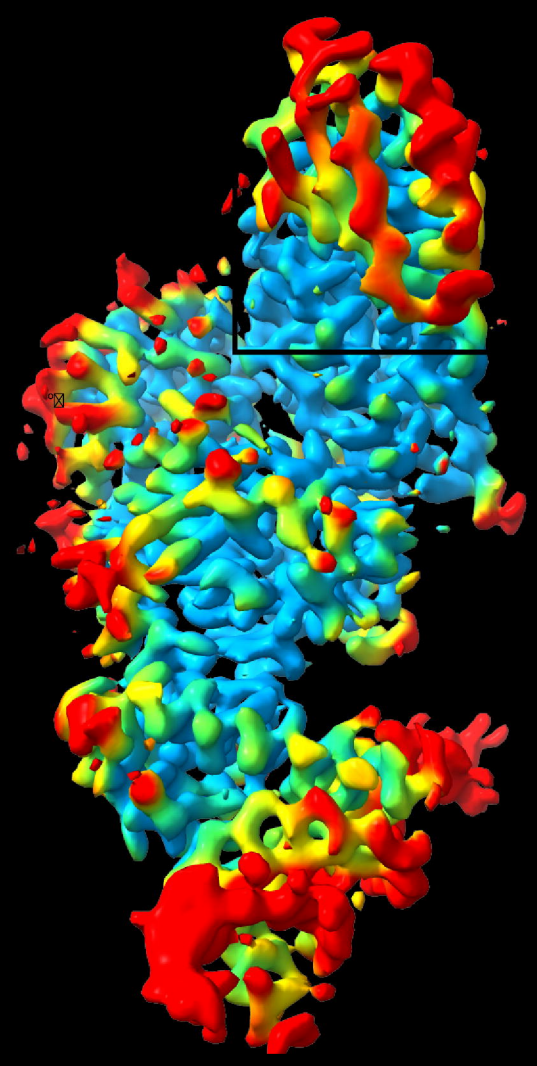

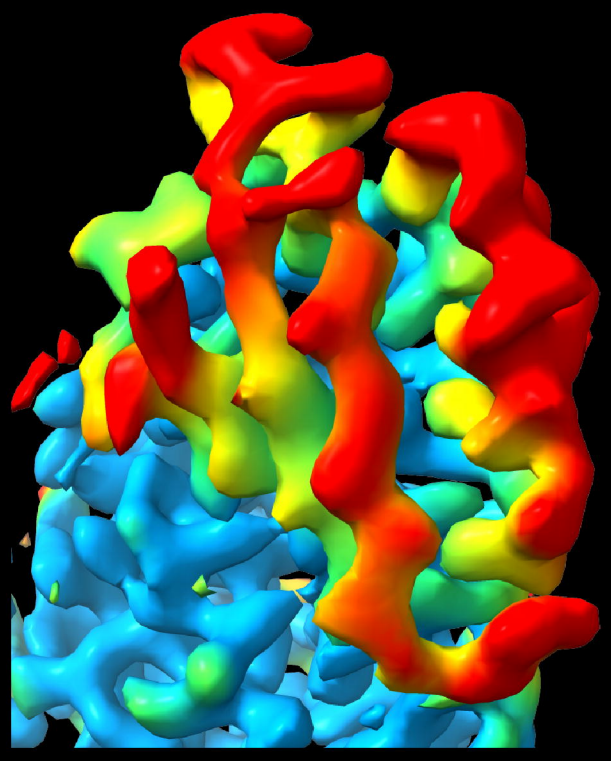

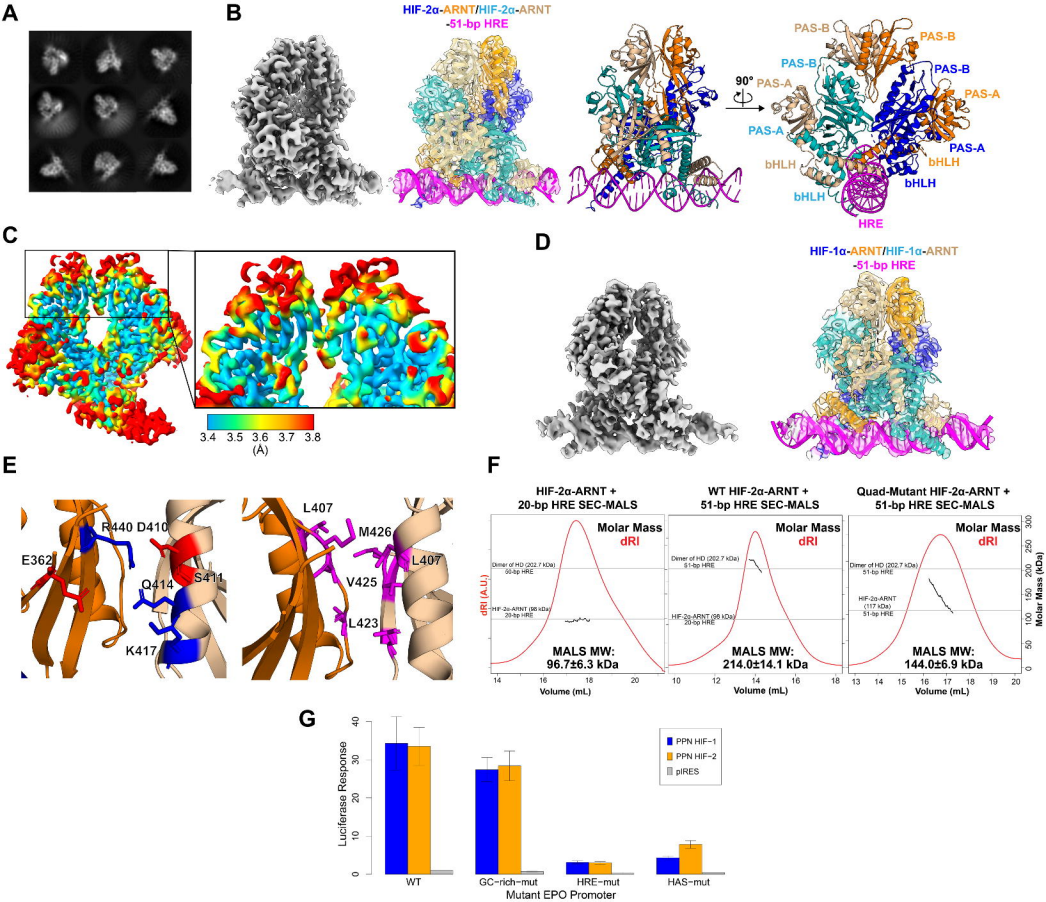
A
B
HIF-2α-ARNT/HIF-2α-ARNT
-51-bp HRE
90°
PAS-B
PAS-B
PAS-B
PAS-B
PAS-A
PAS-A
PAS-A
PAS-A
bHLH
bHLH
bHLH
bHLH
HRE
C
3.4 3.5 3.6 3.7 3.8
(Å)
D
HIF-1α-ARNT/HIF-1α-ARNT
-51-bp HRE
E
R440
D410
E362
Q414
S411
K417
L407
M426
L407
V425
L423
F
HIF-2α-ARNT +
20-bp HRE SEC-MALS
WT HIF-2α-ARNT +
51-bp HRE SEC-MALS
Quad-Mutant HIF-2α-ARNT +
51-bp HRE SEC-MALS
Molar Mass
dRI
dRI (A.U.)
Molar Mass (kDa)
Dimer of HD (202.7 kDa)
50-bp HRE
HIF-2α-ARNT (98 kDa)
20-bp HRE
Dimer of HD (202.7 kDa)
51-bp HRE
HIF-2α-ARNT (98 kDa)
20-bp HRE
Dimer of HD (202.7 kDa)
51-bp HRE
HIF-2α-ARNT
(117 kDa)
51-bp HRE
MALS MW:
96.7±6.3 kDa
MALS MW:
214.0±14.1 kDa
MALS MW:
144.0±6.9 kDa
Volume (mL)
Volume (mL)
Volume (mL)
G
Luciferase Response
PPN HIF-1
PPN HIF-2
pIRES
WT
GC-rich-mut
HRE-mut
HAS-mut
Mutant EPO Promoter

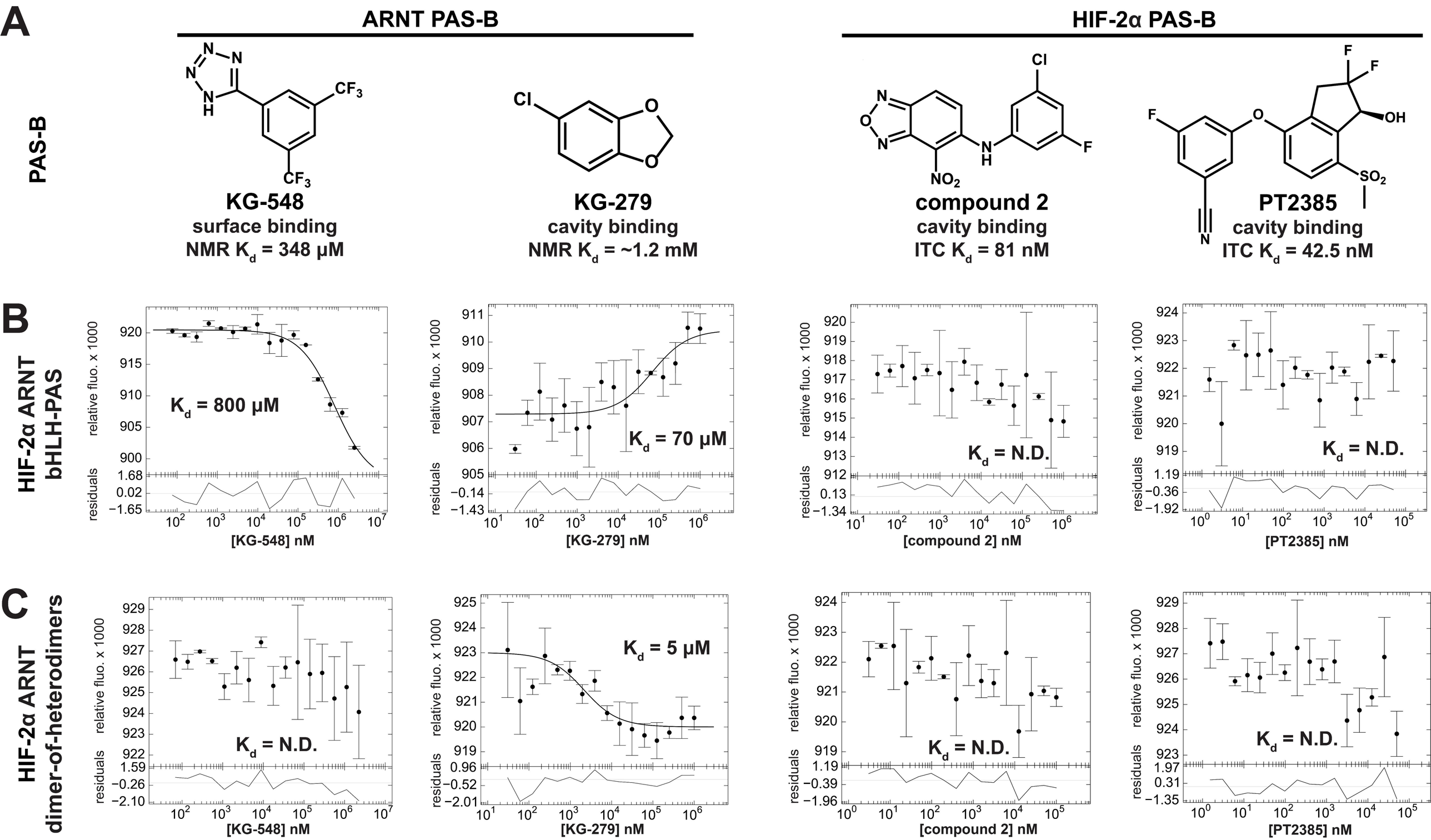
A
ARNT PAS-B
HIF-2α PAS-B
PAS-B
KG-548
surface binding
NMR Kd = 348 μM
KG-279
cavity binding
NMR Kd = ~1.2 mM
compound 2
cavity binding
ITC Kd = 81 nM
PT2385
cavity binding
ITC Kd = 42.5 nM
B
HIF-2α ARNT bHLH-PAS
Kd = 800 μM
Kd = 70 μM
Kd = N.D.
Kd = N.D.
C
HIF-2α ARNT dimer-of-heterodimers
Kd = N.D.
Kd = 5 μM
Kd = N.D.
Kd = N.D.
relative fluo. x 1000
residuals
[KG-548] nM
[KG-279] nM
[compound 2] nM
[PT2385] nM

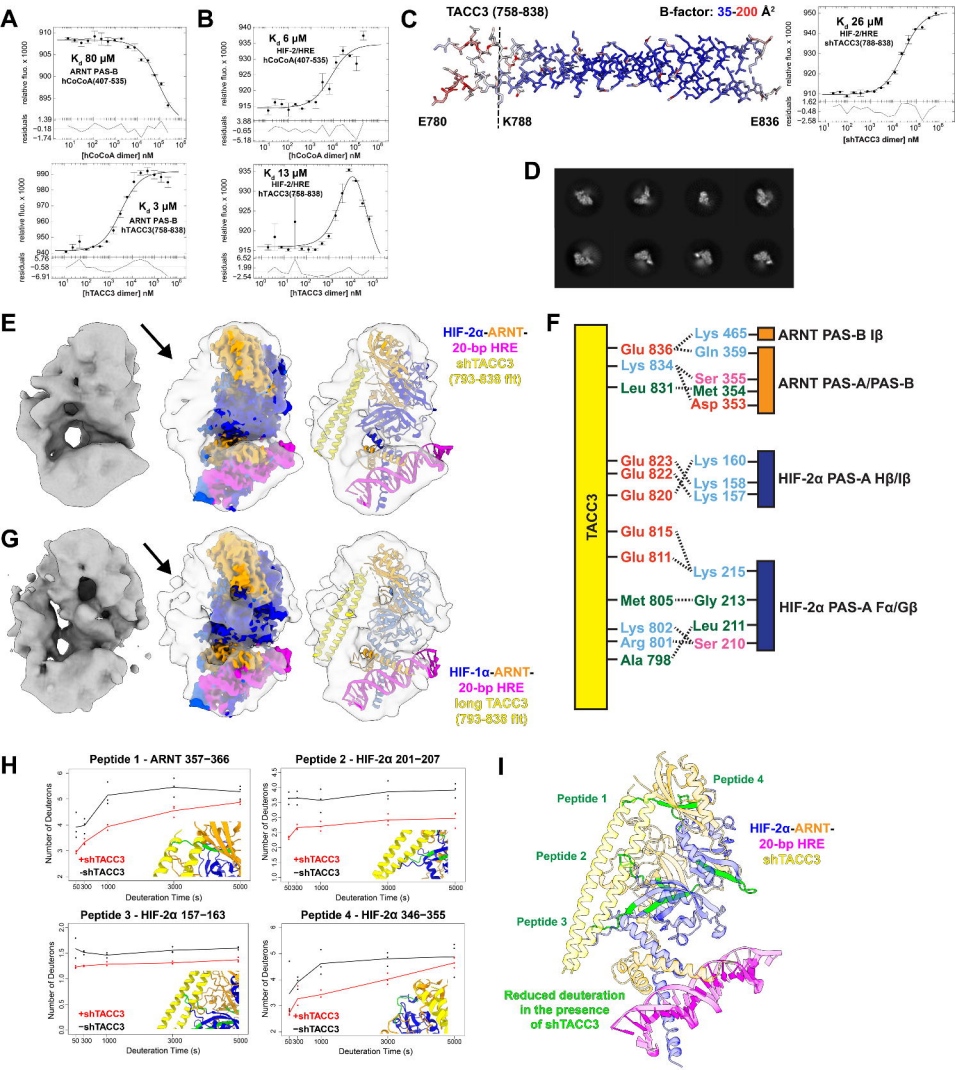
A
K_d 80 µM
ARNT PAS-B
hCoCoA(407-535)
K_d 3 µM
ARNT PAS-B
hTACC3(758-838)
relative fluo. x 1000
residuals
[hCoCoA dimer] nM
[hTACC3 dimer] nM
B
K_d 6 µM
HIF-2/HRE
hCoCoA(407-535)
K_d 13 µM
HIF-2/HRE
hTACC3(758-838)
C
TACC3 (758-838)
B-factor: 35-200 Å²
E780
K788
E836
K_d 26 µM
HIF-2/HRE
shTACC3(788-838)
[shTACC3 dimer] nM
D
E
HIF-2α-ARNT-
20-bp HRE
shTACC3
(793-838 fit)
G
HIF-1α-ARNT-
20-bp HRE
long TACC3
(793-838 fit)
F
TACC3
Glu 836
Lys 834
Leu 831
Lys 465
Gln 359
Ser 355
Met 354
Asp 353
ARNT PAS-B Iβ
ARNT PAS-A/PAS-B
Glu 823
Glu 822
Glu 820
Lys 160
Lys 158
Lys 157
HIF-2α PAS-A Hβ/Iβ
Glu 815
Glu 811
Lys 215
Met 805
Gly 213
Lys 802
Arg 801
Ala 798
Leu 211
Ser 210
HIF-2α PAS-A Fα/Gβ
H
Peptide 1 - ARNT 357–366
Peptide 2 - HIF-2α 201–207
Peptide 3 - HIF-2α 157–163
Peptide 4 - HIF-2α 346–355
Number of Deuterons
Deuteration Time (s)
+shTACC3
-shTACC3
I
Peptide 1
Peptide 2
Peptide 3
Peptide 4
HIF-2α-ARNT-
20-bp HRE
shTACC3
Reduced deuteration
in the presence
of shTACC3

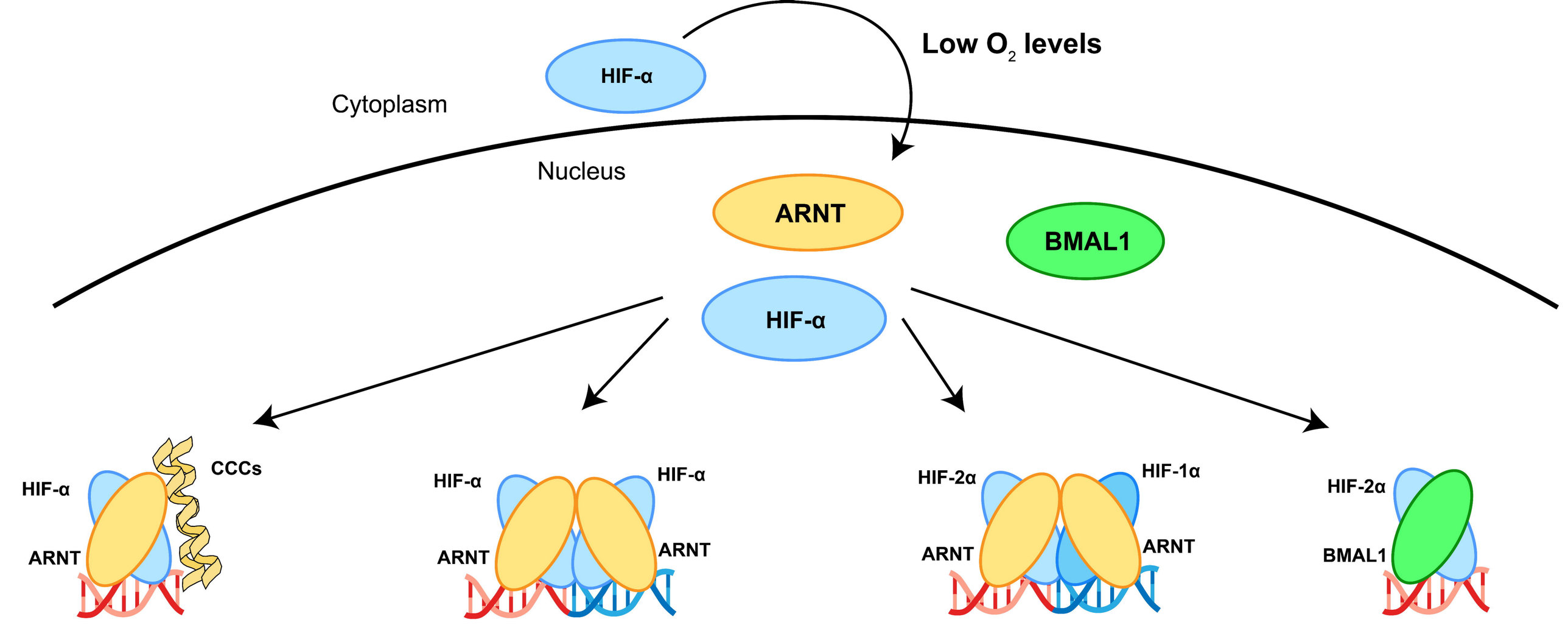

HIF heterodimer

Low HIF-α expression levels

HIF dimer-of-heterodimer

High HIF-α expression levels

HIF-1/HIF-2 *mixed* dimer-of-heterodimer

Pan-HIF crosstalk/regulation

HIF-α/alternative Class II heterodimer

Noncanonical HIF to class II bHLH-PAS protein crosstalk

GLUT1/SLC20A1

...CACGTGGACCGGCTCCCCG...
...GTGCACCTGGCCGAGGGGC...

GAPDH

...TGCGTGCCCAGTTGAACCA...
...ACGCACGGGTCAACTTGGT...

TGFB1

...CGCGTGGGCGGGCTCCGAG...
...GCGCACCCGCCCGAGGCTC...

HRE-only Containing Promoters

EPO

...TACGTGCTGTCTCACACAG...
...ATGCACGACAGAGTGTGTC...

IGFBP2

...GGCGTGCGCGCACTCACTT...
...CCGCACGCGCGTGAGTGAA...

P4HA1

...TACGTGAGCTCGATCACAC...
...ATGCACTCGAGCTAGTGTG...

HRE/HAS Containing Promoters

Novel Routes of Regulation?

- **Differential formation of heterodimer vs. dimer-of-heterodimer as a function of HIF-α expression levels or small molecule inhibitors**
- **Differential recruitment of specific regulatory components by heterodimers vs. dimer-of-heterodimers**
- **HIF-α/ARNT or HIF-α/alternative Class II dimer-of-heterodimer formation**

?